TECHNISCHE UNIVERSITÄT DRESDEN

CBG Max Planck Institute of Molecular Cell Biology and Genetics

DIPLOMARBEIT

zur Erlangung des akademischen Grades

Diplom-Physiker

Investigation of Microtubule Motility Driven by Membrane-Anchored Motor Proteins

vorgelegt von

Janine Fischer

geb. am 23.09.1985 in Magdeburg

angefertigt am

Max-Planck-Institut für Zellbiologie und Genetik, Dresden

Arbeitsgruppe Molekularer Transport

—

Fachrichtung Physik

Fakultät Mathematik und Naturwissenschaften

Technische Universität Dresden

2010

Betreuer:	Dr. Stefan Diez
1. Gutachter:	Prof. Dr. Petra Schwille
2. Gutachter:	Prof. Dr. Jonathon Howard
Eingereicht am:	12. Mai 2010

Eigenständigkeitserklärung

Hiermit versichere ich, dass ich die vorliegende Arbeit ohne unzulässige Hilfe Dritter und ohne Benutzung anderer als der angegebenen Hilfsmittel angefertigt habe. Die aus fremden Quellen direkt oder indirekt übernommenen Gedanken sind als solche kenntlich gemacht. Die Arbeit wurde bisher weder im Inland noch im Ausland in gleicher oder ähnlicher Form einer anderen Prüfungsbehörde vorgelegt.

Dresden, 12. Mai 2010

Janine Fischer

Zusammenfassung

Molekulare Motoren sind Proteine eukaryotischer Zellen, die chemische Energie aus der Hydrolyse von ATP direkt in mechanische Arbeit umwandeln können. Ein solcher Motor ist Kinesin-1, welches innerhalb der Zelle für den aktiven Transport von membranumschlossenen Transportgütern wie Organellen oder synaptischen Vesikeln zuständig ist.

Zur Untersuchung der Kinetik dieser Motoren unter kontrollierten Bedingungen eignen sich zellfreie Minimalsysteme. Viele dieser *in-vitro*-Studien beschreiben die Kraftübertragung einzelner Kinesin-1-Motoren, die mit ihrer Schwanzregion fest an künstliche Transportgüter oder an eine Substratoberfläche gebunden sind und sich mit ihrer funktionellen Einheit entlang von rekonstituierten Mikrotubulifilamenten fortbewegen. Weniger experimentelle Daten gibt es dagegen über das Kollektivverhalten mehrerer Motoren. Dabei sind insbesondere die Transporteigenschaften von membranständigen Motoren interessant, wie es für die Ladungsbeförderung in Zellen von Bedeutung ist.

Im Mittelpunkt der vorliegenden Arbeit steht nun die Frage, ob effektiver Transport durch mehrere Kinesin-1-Motoren möglich ist, wenn diese, entsprechend der *in-vivo*-Situation beim Transport großer Organellen, diffusiv in einer planaren Doppellipidschicht verankert sind. Um dieses Szenario nachzubilden wurden GFP-markierte Kinesin-1 Motorproteine über eine Biotin-Neutravidin-Bindung in Lipiddoppelschichten auf einer Oberfläche verankert und die Lipid-/Kinesindiffusion mit Photobleaching-/ Einzelmolekülmethoden analysiert. Bei hohen Motordichten wurden Gleitgeschwindigkeiten von Mikrotubuli untersucht.

Es wurde festgestellt, dass die Gleitgeschwindigkeiten auf 45 % für sehr hohe bzw. 67 % für mittelhohe Motordichten gegenüber Experimenten mit festem Kinesin reduziert sind. Außerdem wurde ein theoretisches Modell zur Beschreibung des Aufbaus entwickelt, das die verringerten Gleitgeschwindigkeiten durch Diffusion des Lipidankers erklärt. Desweiteren kann aus der Geschwindigkeitsabnahme die Anzahl der wechselwirkenden Motoren pro Mikrotubulilänge vorhergesagt werden.

Abstract

Molecular motors are proteins that are able to convert the chemical energy gained from the hydrolysis of ATP into mechanical work. Among them, kinesin-1 is involved in long-range transport of membrane-enclosed cargo, such as organelles or synaptic vesicles.

The kinetic properties of single kinesin-1 motors have been extensively studied under controlled *in vitro* conditions, where the motors are rigidly attached to an artificial cargo or to a substrate surface, interacting with microtubule filaments. Less is known about the force generation of multiple motors acting in concert. Especially, the collective behaviour of multiple membrane-associated motors is of current interest, such as it known to occur during the transport of membrane-enclosed cargo *in vivo*.

The present study asks, if effective transport by multiple kinesin-1 is possible when the motors are anchored to a planar lipid bilayer in a diffusive manner. This is the case during the transport of large organelles in cells. In order to mimic such a scenario, kinesin-1 motor proteins were anchored to planar supported lipid bilayers via a biotin-neutravidin linkage. The diffusive behaviour of lipid and GFP-labelled kinesin-1 molecules was identified using photobleaching and single molecule imaging techniques, respectively. At high motor density, gliding motion of reconstituted microtubules driven by membrane anchored gliding motor proteins was observed.

It was found that the microtubule gliding velocities are decreased to about 67 % for very high and 45 % for medium high motor density, compared to assays where the motors were rigidly attached to surface-immobilised antibodies. Furthermore, a theoretical model was established for this setup, that describes the decreased gliding velocities as a consequence of the diffusive anchorage of the motors in the lipid bilayer. Additionally, the model allows for a prediction of the number of motor proteins interacting with the microtubule per unit length from the decline of the microtubule velocity.

Contents

Abbreviations and Symbols

Abbreviations

aa	Amino acids.
ADP	Adenosine-5'-diphosphate, a hydrolysed, low energy form of ATP.
AFM	Atomic force microscopy.
ATP	Adenosine-5'-triphosphate, cellular energy unit.
CCD	Charge coupled device, part of a camera.
Da	Dalton, atomic mass unit, commonly used for proteins, $1\,\mathrm{Da} = 1.66 \cdot 10^{-24}\,\mathrm{kg}$.
DiD	1,1'-dioctadecyl-3,3,3',3'-tetramethylindodicarbocyanine, lipid dye analog.
DNA	Desoxyribonucleic acid, bearer of the genetic code in all organisms.
DOPC	1,2-dioleoyl-sn-glycero-3-phosphocholine, typical membrane lipid.
EGTA	Ethylene-glycol-tetraacetic acid, a chelating (two-pronged) molecule used to sequester most divalent metal ions, but with a much higher affinity for calcium than for magnesium.
Fiesta	Fluorescence imaging evaluation software for tracking and analysis.
FRAP	Fluorescence recovery after photobleaching.
GFP	Green fluorescent protein, often used for genetic fluorescent labelling.
GUV	Giant unilamellar vesicle.
KHC	Kinesin heavy chain.
KLC	Kinesin light chain.
MLV	Multilamellar vesicles.
SLB	Supported lipid bilayer.
SPT	Single particle tracking.
SUV	Small unilamellar vesicles.
TIRF	Total internal reflection fluorescence microscopy.

Symbols

D	Diffusion constant in $\mu m^2/s$.
$F(-)$	Fluorescence intensity before bleaching.
$F_K(t)$	Fluorescence intensity recovery evolution for the bleaching parameter K.
$F_K(\infty)$	Fluorescence intensity for $t \to \infty$.
k	Rate, in $1/s$.
K	Bleaching parameter characterising the beam shape.
k_B	BOLTZMANN's constant, $k_B = 1.3806504(24) \cdot 10^{-23}\,J/K$.
M	Molarity, unit of concentrations, in mol/l.
M	Mobile fraction in the FRAP method.
μ	Mobility of a particle.
η	Viscosity of a solution, in $Pa \cdot s$.
R	Radius of the bleaching spot in μm.
T	Temperature in K.
Δt_{frap}	Time interval between two image acquisitions in the FRAP method.
Δt_{spt}	Time interval between different position measurements in the SPT method.
τ_D	Characteristic recovery time.
$\langle \Delta x^2 \rangle$	Mean square displacement of a single particle.

1 Introduction

Among physicists, the 17th century British R. HOOKE is famous for the force law of the HOOKEan spring, whereas for biologists he known as the originator of cell biology. He was the first to use the optical approaches of that time to create a microscope looking for the elements of life. His observations of "little boxes" (lat. cellulae) in thin slices of suberic tissue were published in 1665 in the book *Micrographia* and became popular as the discovery of cells. With the improvement of optical methods, more and more details of (sub-)cellular structures could be resolved, and their functions have been identified over the years. At any time, biological discoveries were strongly coupled with the knowledge of the physical principles of optics that facilitated the immense knowledge of life processes gained up to today. At the end of the 20th century, the application of fluorescence microscopy to biology, in combination with the development of appropriate fluorescent dyes and digital imaging methods, has opened a new area of interdisciplinary research on cellular functions on the nanometre scale.

Nowadays, cells can be described as tiny, highly complex factories comprising different compartments. Each of them fulfils a special function in the ensemble, implying the need of many products to be transported, to keep the departments working efficiently. In eukaryotic cells, long range transport is known to be carried out by motor proteins such as kinesin-1, which was first observed in axons of nerve cells, performing vesicle transport from the cell body to the synapses [Vale et al., 1985]. In the recent years, a whole family of kinesins of various organisms has been identified, and its members are key players in active transport of membrane-bounded cargo as well as in spindle alignment during mitotic cell division [Kim and Endow, 2000, Hirokawa et al., 2009].

Kinesin-1 is known to processively walk along the microtubule filaments at velocities of

800 nm/s, performing discrete 8 nm steps and hydrolysing one ATP[1] per step [Howard et al., 1989, Svoboda et al., 1993, Schnitzer and Block, 1997, Coy et al., 1999, Block et al., 2003]. The analysis of the stepping mechanism, force generation and ATP-hydrolysis of single and kinesin-1 motors was enabled by the use of *in vitro* reconstitution systems that contain only a minimal set of components as shown in figure 1.1.

Gliding assay experiments revealed that, at saturating concentrations of ATP, the microtubule gliding velocities are independent from the microtubule length and from the number of motors propelling the microtubule, for wide ranges of the kinesin density. This led to the assumption that several motors do *not* work in a correlated manner [Howard et al., 1989, Leduc et al., 2007]. Recent studies showed a slow down in the gliding velocity for very high motor densities, indicating slight negative coupling between the motors [Bieling et al., 2008]. Multiple motors pulling a bead have been observed to move with constant velocity when the motor density on the surface of the bead was varied, too, whereby the typical run-length of the bead increased with the motor density [Beeg et al., 2008]. The latter fact would be very helpful for effective long-range transport in cells. However, in *in vivo* experiments from [Shubeita et al., 2008], varying numbers of kinesin-1 motors have been observed to carry lipid droplets at constant run-length, and the transport velocities did not change. Thus, a possible cooperation of multiple motors acting in concert remains an open question in this field.

In contrast to most *in vitro* studies, where the kinesin is rigidly attached to an artificial cargo, the *in vivo* situation comprises a rather soft coupling between several motors, which are attached to membrane-bounded cargo in a diffusive manner. To investigate the kinetics of motors interacting with artificial membranes, kinesin-1 motors have been attached to giant unilamellar vesicles [Leduc et al., 2004]. During this study, the motors were shown to extract membrane tubes off the vesicle by means of the force that was generated while walking along surface immobilised microtubules. The number of interacting motors could be determined by a theoretical model that furthermore revealed a diffusion coefficient of the motors attached to the membrane ($D = 1\,\mu m^2/s$).

It is the aim of the present study to investigate the ability of kinesin-1 motors, which are anchored to a supported lipid bilayer (SLB) via their tails, to propel microtubules through the solution. This is a novel approach to gain a better understanding of the oper-

[1] Adenosine-5'-triphosphate, cellular energy unit.

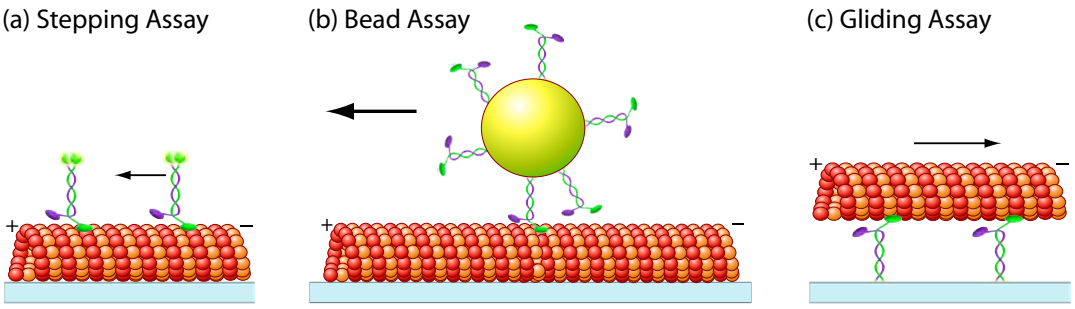

Figure 1.1: Different *in vitro* reconstitution systems to study motor proteins: (a) in stepping assays, microtubules are immobilised at the surface, fluorescently labelled kinesin molecules bind from the solution and can be observed while walking along the fixed microtubules; (b) in the bead assay, kinesin coated beads are pulled towards the microtubule plus-end and the position of the bead is recorded with high precision [Svoboda et al., 1993, Block et al., 2003]; (c) the gliding geometry turns the setup around in such a way that the motors are fixed to the surface by their tails and microtubules binding to the motor domains from solution are propelled over the kinesin coated surface [Howard et al., 1989].

ation of kinesin-1 motor proteins *in conjunction with membrane-bounded cargo*. Thereby, the collective behaviour of several loosely coupled kinesin-1 molecules will be studied. The specific goals are:

- SLB reconstitution in a flowcell system,
- attachment of kinesin-1 motor proteins to the SLB and observation of the diffusive behaviour of the motor proteins at the surface,
- the performance and evaluation of a membrane-anchored gliding assay using biotin neutravidin linkage as is schematically shown in figure 1.2, and
- the theoretical description of the assembly, including the connection to the experimental results.

Therefore, this work is structured as follows. The subsequent chapter 2 provides the basics necessary for the comprehension of this work. It comprises the biological background of the kinesin motor proteins and lipid bilayers as well as the physical principles of diffusion and fluorescence microscopy.

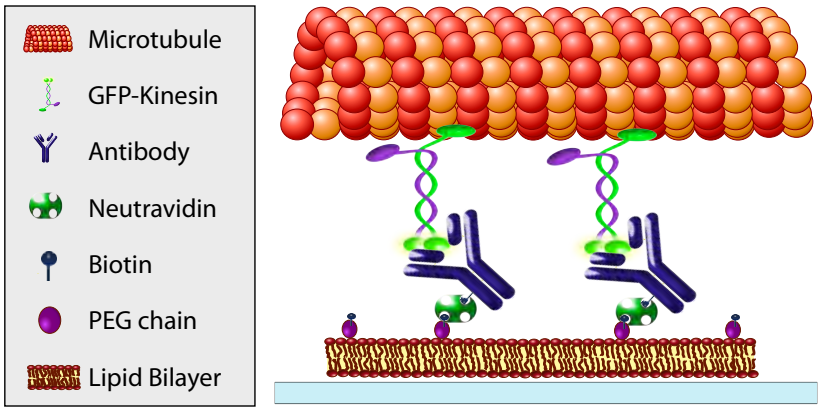

Figure 1.2: Theoretical alignment of the components for the membrane-anchored gliding assay.

In chapter 3, the setup is presented in detail, and a theoretical description of the membrane-anchored gliding assay is derived, for subsequent comparison with the experimental results.

Chapter 4 explains the realisation of the assay, which has been developed based on published protocols for SLB formation and gliding motility assays. Among other things, it will be shown how SLBs can be introduced into a flowcell and how gliding motility was achieved and measured. Furthermore, the fluorescence imaging techniques for single molecule detection will be discussed, as well as the image processing that is required, for the measurement of the diffusion coefficient from fluorescence recovery after photobleaching (FRAP) curves or single particle tracks, and for the determination of the microtubule gliding velocities from image stacks. Altogether, the chapter is showing how the data was generated.

The results of the measurements are presented and discussed in chapter 5, which is separated into the different steps of the assay. First, the SLB formation in the flowcell is discussed on the basis of the obtained diffusion coefficients of the lipids in the SLB. Then, the diffusion coefficient of kinesin anchored to an SLB as measured by FRAP and SPT is considered and judged in conjunction with the theoretical considerations performed in chapter 3. Finally, the results of the microtubule gliding experiments of the complete motility assay are presented. Using the results of the model, the average gliding velocities are related to the density of motors interacting per microtubule length.

The last chapter summarises the achievements of this work and develops prospects for future investigations.

2 Basic Principles

The content of this chapter will bring together the basics of cell biology and the principles of physics that are necessary for the understanding of this thesis. The kinesin-1 motor proteins occupy the pivot position since they act as the driving force in the motility experiments. Therefore, section 2.1 elucidates the operation of cargo transport along the microtubule tracks by the kinesin-1 motors. It will be described that kinesin is able, to perform 8 nm steps by binding alternately to the microtubule with its two motor domains, and to make about a hundred consecutive steps without detaching. Thereby, a single kinesin-1 motor is able to generate forces up to 56 pN, enabling effective transport of large cargo inside cells against the viscous drag of the transport object, which is often considerably larger than the motors themselves. Finally, the manifold mechanisms for the attachment of the cargo to the motors *in vivo* are outlined during this section.

During this study, membrane-bounded cargo is mimicked by lipid bilayers, where motor proteins are anchored to. Therefore, the section 2.2 gives a general introduction to lipid bilayers, from the structure of single lipid molecules, their arrangement in an aqueous environment up to solid supported lipid bilayers. Moreover, the dynamics of membrane lipids in the bilayer are dominated by lateral diffusion, and therefore the knowledge of the physical laws of diffusion is essential for the understanding of the gliding motility experiments to be performed.

In the focus of the section 2.3 is the fluorescence microscopy which is used for visualisation of the different biological components. Thereby, the principles of fluorescence are explained from a quantum mechanical point of view. Furthermore, the fluorescent dye molecules – the fluorophores – are introduced with respect to their classification, properties and limits. In the end, the microscopy techniques necessary for fluorescence detection will be explained, including the total internal reflection fluorescence (TIRF) microscopy facilitating single molecule detection near surfaces.

2.1 Cargo Transport by Kinesin-1 Motor Proteins

Active intracellular transport processes in eukaryotic cells are known to be carried out by molecular motor proteins such as kinesin, dynein and myosin, which are able to walk along filaments of the cytoskeletal network (see figure 2.1). One important component of the cytoskeleton are actin filaments, which are located near the cell membrane and, in conjunction with myosin motors, are responsible for muscle contraction. The other cytoskeletal transport platform for motor proteins is provided by the *microtubules*. They astrally spread from the centrosomes in the microtubule organising center in the nucleic region of the cell to the periphery, and are usually associated with the kinesin and dynein motor proteins.

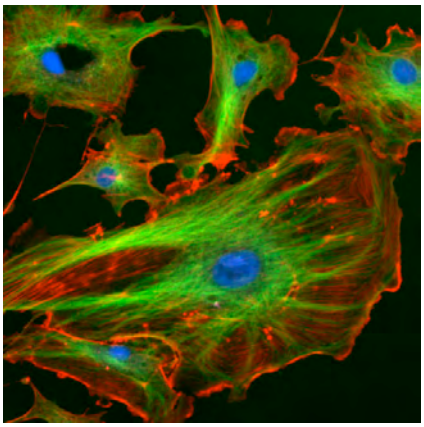

Figure 2.1: Fluorescent cell, red: actin, green: microtubules, blue: DNA. From http://rsb.info.nih.gov/ij/images/FluorescentCells.jpg, last checked on May 7, 2010.

Microtubule Tracks

Microtubules are hollow cylinders with a diameter of 25 nm and a length of up to 100 µm. They polymerise from tubulin dimers which are made of tightly bound α- and β-tubulin [Feit et al., 1971, Wade, 2009]. The dimers build a protofilament with alternating α- and β-subunits, and usually 13 protofilaments[1] form the cylinder (see figure 2.2). The resulting tube has an intrinsic polarity with having an α- and a β-tubulin end. The two microtubule tips have different polymerisation rates, whereby the fast growing plus-end corresponds to the β-end and the slowly growing minus end to the α-end [Desai and Mitchison, 1997]. To prevent depolymerization, microtubules are usually stabilized with taxol in *in vitro* research applications [Schiff et al., 1979].

Due to the polarity of the microtubules, the stepping of motors along the microtubules

[1] The number of "13" protofilaments is the most frequent one in vivo, although numbers of protofilaments from 8 to 20 have been observed as well [Andreu et al., 1992, Alberts et al., 2008].

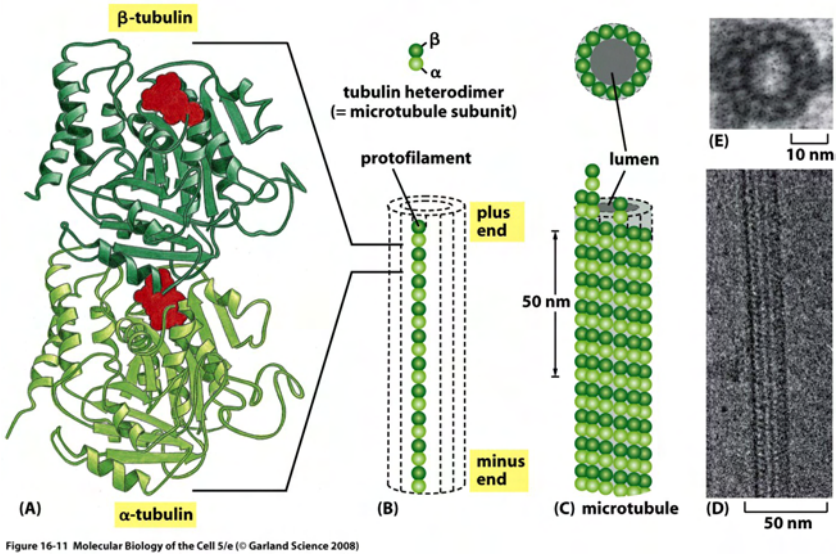

Figure 2.2: Microtubule structure. (A) The tubulin dimer consists of α- and β-subunits. (B) The dimers align lengthwise to form a polar protofilament. (C) The microtubule cylinder is made of several protofilament strains, which can also be seen in the electron microscopy image (D); from [Alberts et al., 2008].

is restricted to one direction, enabling directed transport. Kinesin motors are mostly involved in anterograde transport, which means moving towards the plus-end of microtubules and thus to the periphery of the cell, and thus oppose dynein retrograde transport. Using the ability of kinesins to carry vesicular cargo over long distances, they contribute to specific transport of membrane proteins from the production site near the nucleus to their destination in the plasma membrane as well as positioning of organelles [Kirschner and Mitchison, 1986, Hirokawa et al., 2009]. In addition to cargo transport, kinesin motor proteins are crucial during mitotic cell division, wherein they are involved for remodelling of the cytoskeleton to the spindle as well as the correct separation of the chromosomes [Hayden et al., 1990, Glotzer, 2009].

Structure of the Kinesin Molecular Motors

The intrinsic property of kinesin is a specific motor domain that allows for binding to microtubules and for ATP hydrolysis and enables the conversion of chemical energy into mechanical work. Precisely, there is a whole group of such proteins, the so called kinesin superfamily [Kim and Endow, 2000, Dagenbach and Endow, 2004, Miki et al.,

2005, Hirokawa et al., 2009]. The kinesin superfamily members are different proteins from eukaryotic organisms containing this structurally conserved globular motor domain, which is usually located at the N-terminus of the amino acid sequence[2], but it can also be located at the C-terminus or in the middle. The most prominent representative, conventional kinesin or kinesin-1, has a C-terminal domain causing plus-end directed transport.

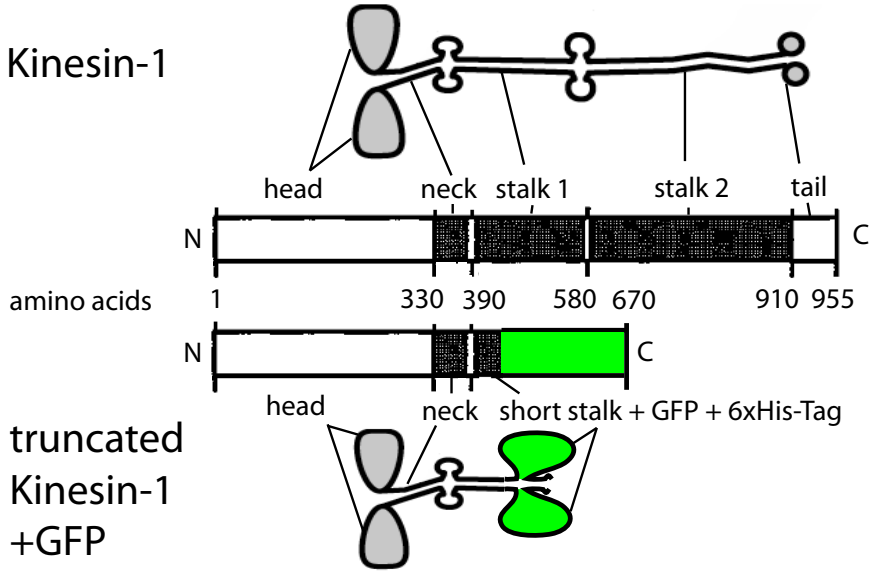

Figure 2.3: Structure of Kinesin-1. Wild-type (upper panel) and truncated GFP-kinesin (lower panel). Modified from [Kozielski et al., 1997].

Like most kinesins, kinesin-1 is a heterotetramer comprising two equal heavy chains (KHC) necessary for walking, and two light chains (KLC), which possess specific cargo binding sites that are discussed later in this section. KHC is a dimer made of two equal 960 amino acid (aa) chains (see figure 2.3). Each heavy chain consists of the N-terminal globular motor domain or *head* that is linked to a short, flexible *neck* linker. The following coiled-coil region, the *stalk*, is responsible for dimerisation. The C-terminal *tail* associates with a pair of KLCs *in vivo*. However, the kinesin used during this study is a truncated version of KHC consisting of the 430 N-terminal amino acids (aa), i.e. leaving the motor domain and a part of the stalk region that still allows the formation of a dimer,

[2]Amino acid sequences are polar. Each amino acid has a carboxylic group ($-COOH$) and an amine group ($-NH_2$) allowing for peptide bond formation ($NH-CO$) plus water. At the end of a sequence of amino acids (which generates a protein), there is always one acid group free naming the end $N-$ or $C-$terminus.

and an additional the 6xHis-tag[3] at the C-terminus as well as the GFP sequence [Rogers et al., 2001]. The tail modification does not affect the walking mechanism.

Kinesin-1 Walking Mechanism and Force Generation

Kinesin-1 is a processive motor, able to perform a hundred consecutive 8 nm steps towards the plus-end of a microtubule, while it is ever following a single protofilament [Hackney, 1995, Ray et al., 1993]. Thereby, the step size corresponds to the distance between two tubulin dimers, i.e. one head binds to exactly one tubulin dimer [Svoboda et al., 1993]. Exactly one ATP is consumed per step, and about 100 ATP get hydrolysed per second at a saturated ATP concentration of about 1 mM, resulting in an average velocity of 800 nm/s [Howard et al., 1989, Schnitzer and Block, 1997, Coy et al., 1999].

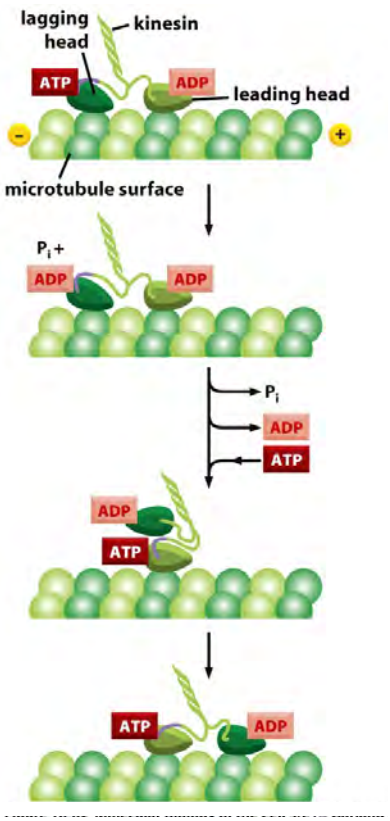

Figure 2.4: Kinesin hand-over-hand walking mechanism. From [Alberts et al., 2008].

The stepping of the two heads is proposed to happen by a coordinated, asymmetric *hand-over-hand mechanism* like illustrated in figure 2.4 [Asbury et al., 2003, Yildiz et al., 2004]. Thereby, one head is always tightly bound to the microtubule, enabling the processivity of the motor. The clue to directed motion lies in the coupling of the two binding sites of the motor domain for ATP and tubulin. When ADP is released at the bound head, and ATP gets to the ATP binding pocket of this head (figure 2.4c), the whole protein undergoes a conformational change to an energetically higher state, providing the energy for the *power stroke*, where the rear head is pulled to the front, meanwhile ATP is getting hydrolysed in the bound head. The novel leading head attaches to the microtubule and after the releasing phosphate and ADP, it can bind fresh ATP and pull the other head to the front in the same manner.

[3]Series of six consecutive amino acids histidine, necessary for protein purification.

The coordination of the two motor domains is thought to be facilitated by internal strain in the neck linker [Yildiz et al., 2008].

By this mechanism, a single kinesin-1 motor is able to walk against load force up to 6 pN, although velocity and run length before detaching from the microtubule decrease with load. This has been shown in optical trapping experiments of a bead attached to kinesin (figure 2.5) and for kinesin motors propelling microtubules under viscous load [Hunt et al., 1994]. Force application in directions perpendicular to the kinesin's drive does not have much effect on the velocity [Block et al., 2003].

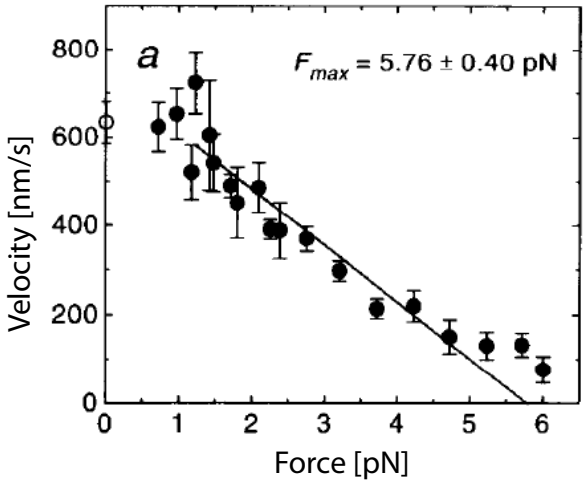

Figure 2.5: Force velocity curves for a single kinesin motor, data points are mean velocities ± the standard error of the mean, the linear fit includes the data from 1.5 to 5 pN. From [Svoboda and Block, 1994].

Using the kinetic properties, it is possible to determine the energy efficiency of a kinesin motor. For each step of 8 nm length under a maximum load of 6 pN, kinesin exerts an energy of $W = 8\,\text{nm} \cdot 6\,\text{pN} = 48 \cdot 10^{-21}\,\text{J}$, i.e. about half of the chemical energy released by the hydrolysis of one ATP-molecule under physiological conditions of $10^{-19}\,\text{J}$ [Bray, 2001]. Hence, kinesin-1 motors have an efficiency of almost 50%, which is much better than the combustion engines in cars ($\approx 35\%$).

Cargo Attachment and the Transport Specificity *in vivo*

Inside cells, the kinesin motors actively transport membranous vesicles, organelles or protein complexes to their destination, which is illustrated in figure 2.6. The attachment of cargo to kinesin-1 is mediated via the tail region of KHC (figure 2.3) in combination with the associated KLC, whereby the light chains are thought to be responsible for the specificity of the interaction [Karcher et al., 2002, Hirokawa and Noda, 2008].

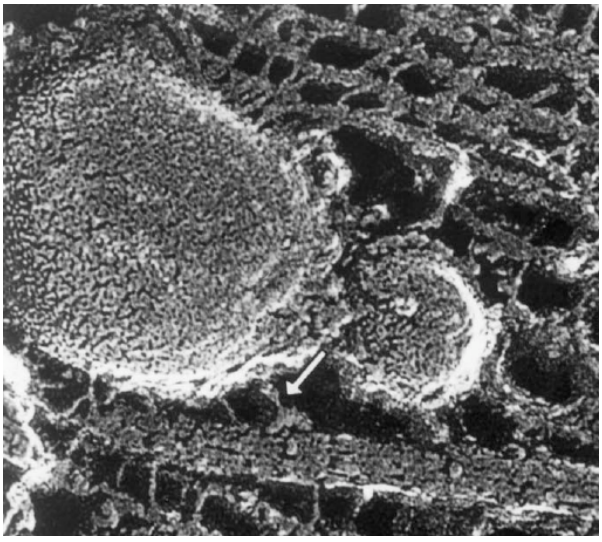

Figure 2.6: Kinesin is carrying an organelle along the microtubules of an axon. Electron micrograph obtained by quick-freeze, deep-etching techniques, image size 350 x 350 nm, from [Hirokawa and Noda, 2008].

The first direct interaction of kinesin was reported for *kinectin*, a large integral ER membrane protein, which was thought to be the universal kinesin anchor [Toyoshima et al., 1992], but whose importance was constrained by the identification of further interactions. For example, in neuronal cells KHC was found to bind directly to the synaptosomal-associated-protein-25, which is part of an integral membrane protein complex in synaptic vesicles. Furthermore, the mitochondria-associated protein *milton* is proposed to be required for kinesin-mediated transport of mitochondria to nerve terminals [Stowers et al., 2002].

Cargo molecules that bind directly to KLC have also been identified. Therefore, a tetratricopeptide repeat domain of KLC has been reported to be a possible binding site. Exemplarily for indirect interactions mediated by the KLC is the attachment of vesicles

containing the amyloid precursor integral membrane protein, which is involved in the regulation of synapse formation, or the connection of KLC to a receptor called ApoER2 via a scaffolding protein known as c-jun-N-terminal-kinase interacting protein [Hirokawa and Noda, 2008].

Although several of these specific interactions have been reported, cargo attachment seems to imply a whole complex of regulatory mechanisms and many relations are far from being fully understood. However, it is an accepted fact, that among the kinesin family, the variety of the transport tasks carried out by different kinesin motors is facilitated by the structural differences in the tail region. This is in contrast to the dynein motor, where the dynein-dynactin complex uses a complicated regulatory mechanism to adapt to specific requirements of a cargo and the scaffold structure of the motor is conserved over a variety of organisms [Mallik and Gross, 2004].

2.2 Lipid Bilayer Systems and Diffusion

All kinds of cells possess flexible membranes to keep reaction volumes separated. Because of this separating function, membranes are believed to have been one of the essential requisites for the first organisms being formed out of the primordial soup. The complex membranes in cells consist of a bilayer of membrane lipids in order to create well separated reaction volumes. Furthermore, they contain different kinds of proteins and saccharides, which can either be integrated into the lipid bilayer or peripherally attached to it. These components are involved in a variety of signalling and transport processes associated with the membrane. During this work, an artificial *in vitro* reproduction of the lipid bilayer, made up of pure lipids without further biomolecules was used.

Structure of Membrane Lipids

A lipid molecule consists of a glycerol backbone that has three hydroxyl groups as binding sites for fatty acids. In *phospholipids*, which are typical membrane lipids, two of these binding sites are occupied by unpolar hydrocarbon chains, while the third binding site is associated with a phosphate group as a linker for the polar head (see figure 2.7). As a

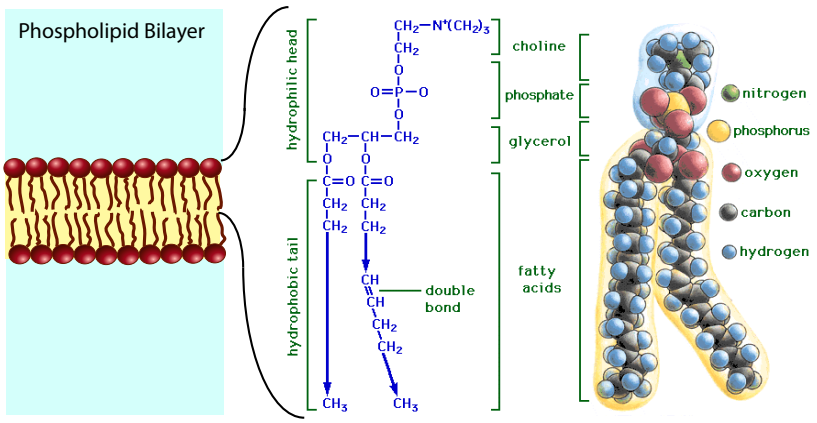

Figure 2.7: A phospholipid bilayer is composed of amphiphilic phosphatidylcholine (PC) molecules, which is presented in chemical formula in the centre and in space-filling model to the right. Modified from [Martin, 2007].

consequence, the molecule is split into two basically different domains: The polar head region which tends to form hydrogen or electrostatic bonds with likewise polar water molecules. It is therefore named *hydrophilic*. In contrast, the unpolar hydrocarbon chains try to avoid contact with polar structures for energy minimisation. They build the *hydrophobic* part of the molecule. According to the property of unifying these two regimes in one molecule, the membrane lipids are called *amphiphilic*. The overall size of a phospholipid molecule is about 3 nm in length and the membrane surface area occupied by one molecule was determined to be $< 1\,\mathrm{nm}^2$ [Engelman, 1969, Nagle and Tristram-Nagle, 2000].

Lipids in Aqueous Environment

When the membrane lipids are brought into contact with water, they immediately arrange in a way that all the heads face the water molecules and the tails point in the opposite direction. Together with a second layer of hydrophobic tails upside down, a double layer of ordered lipids spontaneously forms. This was first suggested by Langmuir in the beginning of the 20th century, and was later confirmed by Gorter and Grendel [Gorter and Grendel, 1925]. To reduce the contact surface of polar and unpolar regions, different lipid bilayer structures can be formed (see figure 2.8).

The most common form is a closed bilayer vesicle, since the edges of planar bilayers

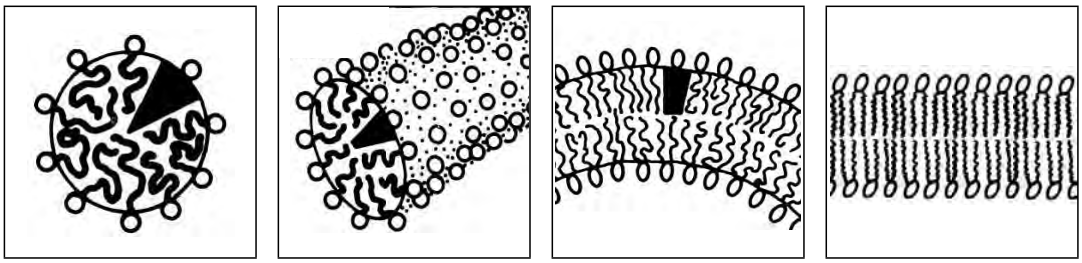

(a) Micelle. **(b)** Tube. **(c)** Vesicle. **(d)** Planar bilayer.

Figure 2.8: Bilayer structures. Modified from [Israelachvili, 1992, p. 344].

are very unstable. Different types of vesicles are distinguished with respect to their size and to the number of bilayers in the structure. For instance, giant unilamellar vesicles (GUVs) have a diameter of several micrometres and are bounded by a single bilayer. The small unilamellar vesicles (SUVs) with a diameter $< 100\,\text{nm}$ also possess a single bilayer. Probes of vesicles with different size and several bilayers are called multilamellar vesicles (MLVs). The exact and energetically most favourable shape of the bilayer depends on the system properties like pH, ionic strength and the lipid content in the solution, but also on the shape of the lipids themselves. For example, lipids with especially short hydrocarbon chains prefer to build small vesicles compared to long, straight molecules. In cells, an immense variability of lipids and membrane proteins enables the separation of reaction sites for all kinds of bilayer structures, from the tiny transport droplet to whole organelles with complex membrane systems like mitochondria.

On the other hand, special treatments can also influence lipid bilayer shape. For example, vesicles that adhere to a strongly hydrophilic and negatively charged surface can be destabilised by the addition of Ca^{2+}-ions to the solution or by a change of the pH. The consequently induced vesicle rupture is used to generate a planar form of a lipid bilayer close to a surface, which is known as the *supported lipid bilayer* (SLB).

Supported Lipid Bilayers

The historically grown method for SLB preparation is the Langmuir-Blodgett method, which comprises the sequential stacking of lipid monolayers formed at a water-air interface. However, the research on SLBs was pushed by the invention of the more handy

method using the vesicle adhesion and rupture on silica surfaces [Brian and McConnell, 1984]. This method was found to work especially well on mica[4] surfaces [Reviakine and Brisson, 2000, Benes et al., 2002], but glass can be used as well, when it is properly treated [Johnson et al., 2002, Schönherr et al., 2004].

SLBs on a mica surface are located on a thin water layer of about 1 nm thickness, which is established between the surface and the lipids of the bilayer, due to electrostatic interactions [Richter et al., 2006]. Because the bilayer is stabilized by the close interaction with solid support, SLBs are easier to handle than free standing bilayers and have become a powerful tool to study membrane associated problems. Furthermore, it enables bilayer observation by surface related techniques such as atomic force microscopy (AFM) or total internal reflection fluorescence (TIRF) microscopy. SLBs were used in the present study, as a tool to anchor kinesin motor proteins and investigate microtubule motility in this conformation. A detailed protocol for the preparation of SLBs is given in section 4.2.

Lateral Diffusion in Membranes

The behaviour of lipids in biological membranes can be explained by the *fluid mosaic model*, which was established by Nicolson and Singer in 1972. It suggested that the components of biomembranes, lipids and proteins, can easily switch positions with neighbouring molecules within a monolayer. Thus, they move more or less freely in the two dimensions of the bilayer, the process of which is called *lateral diffusion*. In contrast, the translational exchange of lipid molecules between the two bilayers, referred to as *flip-flop*, is extremely seldom, since the hydrophilic head group of the lipid molecule would have to cross the hydrophobic core region of the bilayer. Further possible motion modes are the rotation of lipid molecules around the length axis and the flexion of the hydrocarbon chains against each other.

However, the most important process is lateral diffusion, which is caused by the collisions of the lipid molecules in the bilayer due to their thermal fluctuations. That means, the lateral diffusion is a consequence of the two-dimensional Brownian motion.

[4] *Mica* is a sheet silicate with multiple applications due to its nearly perfect cleavage along a crystal axis and to the very flat surface of the sheets.

Diffusion Processes in Lipid Bilayers

BROWNian motion can be microscopically modelled by a random walk of a particle moving with a fixed step size Δx and a rate $1/\Delta t$. It results, that the average displacement $\langle \Delta x \rangle$ of a randomly stepping particle equals zero, but the mean square displacement $\langle \Delta x^2 \rangle$ is proportional to Δt via

$$\langle \Delta x^2 \rangle = 2d \cdot D \cdot \Delta t, \tag{2.1}$$

with the diffusion coefficient D acting as a proportionality constant, and d being the dimension of the particle motion. For the lipid diffusion in the lipid bilayer, $d = 2$ applies, leading to

$$\langle \Delta x^2 \rangle = 4 \cdot D \cdot \Delta t. \tag{2.2a}$$

Equation (2.2a) describes the free, two-dimensional diffusion of a single molecule without external constraints. Assuming a constant flow of a velocity v_0 brings up an extra term to the displacement $\langle \Delta x \rangle = v_0 \cdot \Delta t$ that adds to the mean square displacement as well:

$$\langle \Delta x^2 \rangle = 4 \cdot D \cdot \Delta t + v_0^2 \cdot \Delta t^2. \tag{2.2b}$$

In real bilayers, there might be objects hindering the free diffusion of such a particle, for example static or slowly diffusing "rocks" in the fluid. The particle motion in the presence of these objects is called *anomalous subdiffusion* [Feder et al., 1996, Schwille et al., 1999] and yields a non-linear dependence of $\langle \Delta x^2 \rangle$ on Δt like

$$\langle \Delta x^2 \rangle \sim \Delta t^\alpha \qquad \text{(whereby } 0 < \alpha < 1\text{)}. \tag{2.2c}$$

A further constraint of the diffusing molecule to a limited area is known as *corralled diffusion*, which has been reported for membrane lipids as *lipid rafts* [Simons and Ikonen, 1997, Fujiwara et al., 2002, Niehaus et al., 2008].

The different relations between $\langle \Delta x^2 \rangle$ and Δt are plotted in figure 2.9. Thus, the diffusion type can be determined from the behaviour of the mean square displacement of a single diffusing particle.

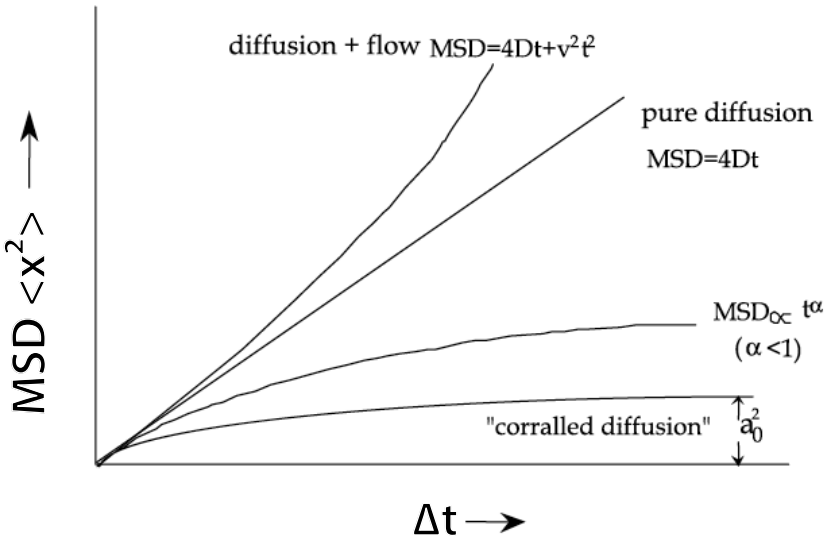

Figure 2.9: Theoretical curves of the mean square displacement (MSD) for a two-dimensional motion of a particle, versus the time interval of the displacement for pure diffusion with/without collective displacement caused by a constant flow of a velocity v_0, anomalous subdiffusion and corralled diffusion (restricted to a circle disc of radius a_0). Modified from [Chen et al., 2006].

Einstein-Smoluchowski Relation

The recent description of single particle diffusion has used a microscopic approach using the characteristic quantity $\langle \Delta x^2 \rangle$. But diffusion can also be described from a macroscopic point like in the FICK law of diffusion relating the flux J to the spatial concentration gradient. The diffusion coefficient D was found to connect these two worlds via the following relation found by EINSTEIN and SMOLUCHOWSKI:

$$\frac{D}{\mu} = k_B T \tag{2.3}$$

and

$$\mu = \frac{v}{F} \tag{2.4}$$

Lipid Composition	Support	D in $\mu m^2/s$	Source/Method
DOPC, 0.5 mol% NBD-PC	glass, detergent cleaned	7.1 ± 0.1	[Seu et al., 2007] by FRAP
DOPC, 0.5 mol% NBD-PC	glass, detergent cleaned, piranha-etched	$(7.9-9.8)\pm0.1$	[Seu et al., 2007] by FRAP
DOPC, 0.5 mol% NBD-PC	glass, detergent cleaned, baked	3.1 ± 0.1	[Seu et al., 2007] by FRAP
80% DOPC, 20% DOPS, 1:100,000 labelled lipids	mica	$(2.0-2.8)\pm0.5$	[Benes et al., 2002] by FCS

Table 2.1: Diffusion coefficient D in different conditions.

with D... diffusion coefficient in $\mu m^2/s$;
μ... mobility a particle in N·s/m;
k_B... BOLTZMANN's constant, $k_B = 1.3806504(24) \cdot 10^{-23}$ J/K;
T... absolute temperature in K;
v... drift velocity of a particle to an applied force in m/s; and
F... force to a single particle in N.

That means, besides the temperature T, D is only effected by the mobility of the lipids μ, which is a consequence of lipid structure and surrounding medium. In case of SLBs, μ is furthermore influenced by the properties of the solid support like charge, hydrophobicity or surface texture as well as the bilayer preparation method itself. For membrane lipids in supported lipid bilayers, D is in the range of several $\mu m^2/s$, whereby $D = 1\,\mu m^2/s$ means that a molecule diffuses about $2\,\mu m$ in a second. Literature values for diffusion coefficients under different conditions are specified in table 2.1. Note that, in contrast to free-standing planar bilayers, D is reduced in SLBs due to an additional friction term arising from the interaction with the surface [Sackmann, 1996, Sonnleitner et al., 1999].

Lipid Bilayer Phases

There are several lipid phases known to occur in natural and artificial lipid bilayers. In a monomolecular bilayer, the phases are distinguished by a transition temperature T_m, which is characteristic for a lipid. The *liquid* and *gel* phase differ in the packing states of

the lipids in the conformational order of the hydrocarbon chains and in the translational order allowing for lateral diffusion [Vist and Davis, 1990, Baumgart et al., 2007]. The addition of cholesterol is proposed to uncouple the transition between conformational and translational order and brings up another separation between *liquid ordered* and *liquid disordered* phase [Nielsen et al., 1999] as shown in figure 2.10. The different phases may vary, for example, in their diffusion constant, thickness and/or surface area per lipid molecule.

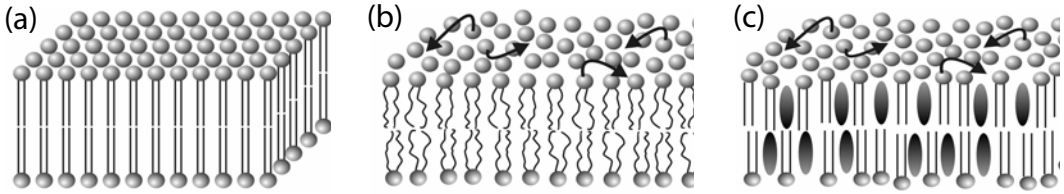

Figure 2.10: Lipid phases, (a) gel phase: straight lipid tails and well-ordered head groups indicate both conformational and translational order, (b) liquid-disordered phase: the phospholipids are in both conformational and translational *dis*order, and (c) liquid-ordered phase: lipid chains are ordered due to interaction with cholesterol (ellipses), but there is translational disorder. Adapted from http://www.biotec.tu-dresden.de/cms/fileadmin/research/biophysics/practical_handouts/guv.pdf, last checked on Feb 12, 2010.

The SLBs used during this thesis mainly were mainly composed of DOPC[5] lipids, which have $T_m = -19\,^{\circ}\mathrm{C}$. Thus, they are is liquid disordered phase and were not expected to show phase separation effects.

2.3 Fluorescence Microscopy

Principle of Fluorescence

The lowest electronic transitions of an organic molecule between the ground state S_0 and the first excited state S_1 are depicted in the JABLONSKI diagram in figure 2.11. In addition to the electronic states, a variety of vibrational states are available and overlay with the electronic ones. At room temperature, the thermal energy does not allow the

[5] 1,2-dioleoyl-sn-glycero-3-phosphocholine, a typical phospholipid used for SLBs, see section 4.1.

excitation of vibrational states, and therefore the molecules are usually in the lowest vibrational level of the ground state S_0.

The excitation of an electron with an energy enabling an electronic transition will lift the electron to the first electronically excited state S_1. Thereby, the final state is usually an excited vibrational state. This process happens in the order of 10^{-15} s. The electron will relax to the vibrational ground state of S_1 within 10^{-12} s.

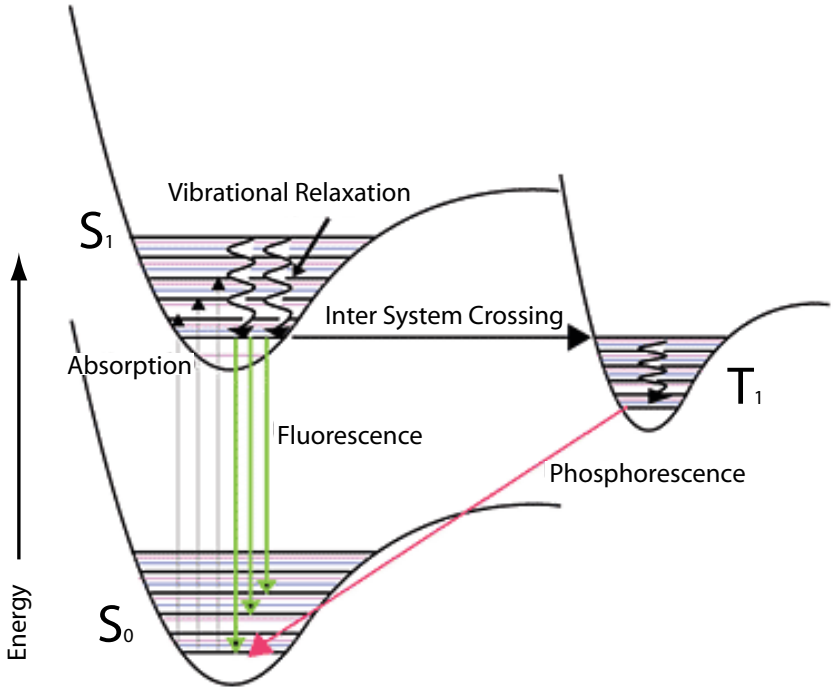

Figure 2.11: JABLONSKI energy diagram of the different electronic transition pathways between the ground state S_0 and the lowest electronically excited state S_1. Relaxation from S_1 may either happen directly, with emission of a photon (fluorescence) or without (non-radiative transition, not shown). The "forbidden" transition refers to an indirect de-excitation of the electron by non-radiative inter system crossing to the T_1 triplet state and, from there, by emission of a photon (phosphorescence) or without (non-radiative transition, not shown) to the ground state. Adapted from http://www.rockefeller.edu/spectroscopy/flouresence2_pop.php, last checked on Jan 14, 2010.

The relaxation of the first excited state S_1 to the ground state S_0 by emission of a photon is called *fluorescence*, whereby the typical lifetime of S_1 is in the order of 10^{-8} s. As can be seen from the JABLONSKI diagram (figure 2.11), the energy of the emitted photon

is slightly lower (or the wavelength is longer) than of the absorbed photon. The energy dissipates due to the fast vibrational relaxation in the S_1 state after absorption as well as to the fluorescence decay to higher vibrational levels of S_0. The effect is known as STOKES *shift*. Further, non-radiative transitions are possible via collisions or conversion to heat.

Besides the mentioned relaxation types, there is a non-zero possibility for the electron to make a "forbidden" transition. In this case, the antiparallel spin (S = 0) of the electron couple is flipped, resulting in the spins of excited and ground state electrons being parallel (S = 1). The process of the electron spin change is called *inter system crossing*. Introduced into a magnetic field, the molecule shows three different eigenstates for the spin (-1, 0 and 1) and the state is therefore called *triplet* state T_1, in contrast to the *singlet* state having only one possible orientation. From the T_1-state, the molecule can only relax to S_0 by another inter system crossing transition. In case that this transition is accompanied by the emission of a photon, it is called *phosphorescence*. Due to the low probability of the process, the T_1-state has a very long lifetime compared the direct relaxation to the electronic ground state, ranging from milliseconds to seconds.

Fluorescent Probes

In most atoms, the excitation energy of the first electronic transition is usually in the range of X-rays. In contrast, fluorophores posses delocalized electrons in a conjugated π-electron system, where the energy level of the first excited state of the molecule is low enough to be excited with visible light. Fluorophores are divided into two classes — intrinsic and extrinsic ones. Intrinsic fluorophores occur naturally (e.g. aromatic amino acids or chlorophyll), which means fluorescence is a natural property of the molecule. Accordingly, extrinsic probes are added to the sample to provide fluorescence when none exists, e.g. fluorescein or rhodamine dye molecules [Lakowicz, 2006, p. 63]. The latter was used for microtubule labelling during this work. Another extrinsic fluorophore that was used during this study is the far red dye DiD[6]. It is a representative of the DiI-family[7] of dialkylcarbocyanines that are utilised for labelling of lipid bilayers, where the water-insoluble fluorophores integrate into the nonpolar regions of the lipid bilayer.

[6] 1,1'-dioctadecyl-3,3,3',3'-tetramethylindodicarbocyanine.
[7] Dialkyl indiocarbocyanine family, lipid dye analogues with similar structure and different wavelength.

In the last decades, intense efforts have been made to identify a variety of fluorescent probes and characterise them by their emission and absorption spectra. An important addition to the library of fluorescent probes was discovery of the *green fluorescent protein* (GFP) from the bioluminescent jellyfish, whose development was honoured with the Nobel Prize to Shimomura, Chalfie and Tsien in 2008. The gene of this protein can be introduced into the gene sequences of other proteins in the cell and subsequently will be expressed with a GFP attached [Chalfie et al., 1994]. The GFP-kinesin used in this work has been labelled by this technique. Altogether, GFP is a powerful marker of gene expression *in vivo* [Rizzuto et al., 1995, Nowotschin et al., 2009].

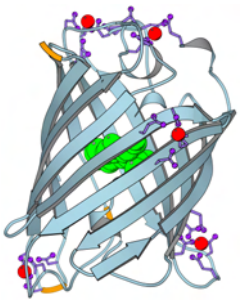

Figure 2.12: Ribbon diagrom of GFP with the photoactive region in the centre. From http://chemistry.gsu.edu/faculty/Yang/Sensor.htm, last checked on Jan 15, 2010.

Quantum Efficiency and Photobleaching

One of the most important properties of a fluorophore is the amount of fluorescent light that can be emitted. This is quantified in the quantum yield q, defined by:

$$q = \frac{k_\gamma}{k_\gamma + k_-}, \tag{2.5}$$

with k_γ being the fraction of de-excitations that lead to the emission of photons, and k_- representing the non-radiative transitions.

The quantum yield q of a fluorophore may strongly depend on the environmental conditions. The inversion of this principle can be used for sensing applications, e.g. to measure changes in pH or rotational diffusion [Lakowicz, 2006, p.63].

Unfortunately, all organic fluorophores show a decay of emission intensity when being illuminated over a certain time. This *photobleaching* effect is especially critical in fluorescence microscopy with high illumination intensities: As a result of strong light excitation, the fluorophores form radicals that can react with oxygen from the solution

and cause a radical chain reaction damaging the fluorophores. For stabilising the fluorophores, oxygen and radical scavenger systems, or *antifade* solutions, comprise glucose and glucose oxidase that reduce the amount of free oxygen in solution. Adding DTT[8] or BME[9] helps in avoiding the radical chain reactions. Like this, photobleaching and protein damage can be effectively reduced. That is especially important when single molecules shall be observed.

Fluorescence Microscopy Techniques

In contrast to a conventional optical light microscope, a fluorescence microscope possesses a dichroic mirror, that allows the separation of excitation and emission light by reflection or transmission of light according to the wavelength of the light. Used in this work was a fluorescence microscope in the inverted setup, the light path of which is shown in figure 2.13. The specimen is illuminated using either a laser or an arc-lamp. The illumination light passes a long-pass excitation filter that selects the short wavelengths necessary for fluorescence excitation. The beam then encounters the dichroic mirror that reflects the excitation light. In the objective, the beam is focussed onto the specimen, where the excitation light is absorbed and fluorescence is induced. The emitted light is collected in the same objective and passes the dichroic mirror, since it has longer wavelengths. After passing the emission filter, it can be observed in the eyepiece or recorded by a charge coupled device (CCD) camera.

A super-resolution technique useful for the observation of single fluorescent molecules located very near to a substrate surface is *total internal reflection fluorescence* (TIRF) microscopy, the principle of which is depicted in figure 2.14. A light beam that encounters an interface to a medium of lower refractive index is totally reflected, when the incident angle exceeds a certain value. As a consequence, there is an evanescent field that penetrates the optically thinner medium and decays exponentially with the distance to the interface. Only fluorescent molecules located very close to the interface (penetration depth about 200 nm) may be excited by the evanescent field. Hence, the background fluorescence from molecules out of the focus is strongly reduced, improving the discrimination of fluorescent molecules close to the surface compared to standard or

[8] 1,4-Dithio-DL-threitol.
[9] Bovine microvascular endothelial.

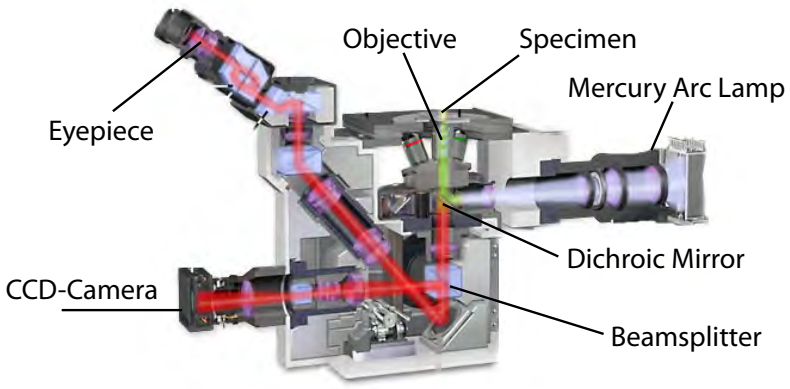

Figure 2.13: Optical setup for an inverted fluorescence microscope illuminated by an arc-lamp. Modified from http://micro.magnet.fsu.edu/primer/techniques/fluorescence/anatomy/ix70fluorescence.html, last checked: Jan 22, 2010.

epi-fluorescence illumination.

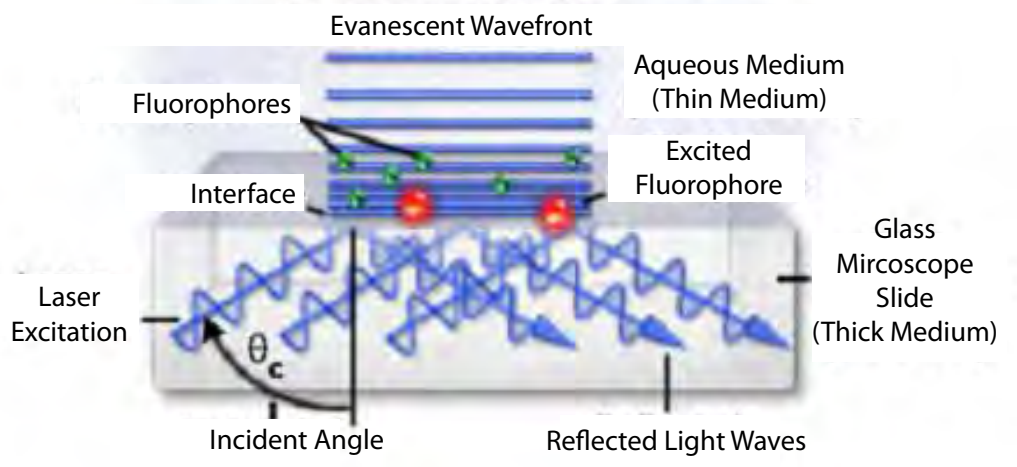

Figure 2.14: Concept of total internal reflection fluorescence (TIRF) microscopy. Incident light waves get totally reflected at an interface of different refractive indices, and the evanescent field can excite fluorophores in the optically thinner medium. Adapted from http://www.chem.iitb.ac.in/~arindam/projects.html, last checked Jan 15, 2010.

3 Theoretical Considerations

The present chapter aims for a theoretical description of the nanoscopic setup used during this study. It shall investigate the dynamic behaviour of the motors and the microtubules in the membrane-anchored gliding assay. In particular, the size extensions of GFP-kinesin-1 (in the following termed *kinesin*) and its anchoring modules are analysed in section 3.1. Based on these parameters, the dynamics of the assay are derived theoretically in section 3.2. Thereby, the central question in this setup is, whether kinesin is able to propel microtubules in spite of its "slippy" anchor in the supported lipid bilayer (SLB). To address this question, the friction forces acting on the different components are analysed in the equilibrium of forces. Consequently, kinesin diffusion in the membrane as well as the dependencies of the microtubule gliding velocity on the length of the microtubule and on the density of motors interacting with the microtubule are predicted in section 3.3.

3.1 Nanoscopic Setup

The theoretical alignment of the components is schematically shown in figure 3.1 for the two kinds of gliding assays used. In the *membrane-anchored gliding assay* (figure 3.1a), the kinesin is anchored in the fluid SLB by a neutravidin-biotin linkage. In contrast, in the *antibody gliding assay*, which was used as a control assay, the kinesin molecules stick to the rigid glass-surface (figure 3.1b).

In the membrane-anchored gliding assay, the SLB has a thickness of 6 nm, and is separated from the surface by a 1 nm water layer. The bilayer is designed to contain a certain ratio of functional lipids with a PEG-biotin cap. Biotin is a vitamin with an exceptionally high affinity to the protein avidin, (dissociation constant $k_D \approx 10^{-14}\,\mathrm{M}^{-1}$,

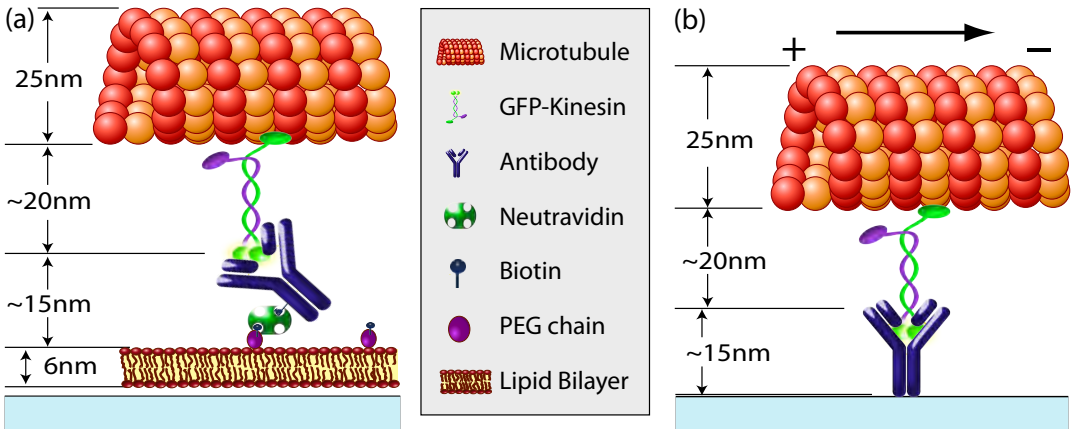

Figure 3.1: Nanoscopic view of the used setups, (a) membrane-anchored gliding assay, and (b) antibody gliding assay (control with antibody immobilised kinesin).

depending on environmental conditions [Merkel et al., 1999]). Therefore, biotin and the deglycosylated avidin relatives *streptavidin* and *neutravidin* are commonly applied as strong, non-covalent linkers in bionanotechnology [Laitinen et al., 2006, Korten and Diez, 2008]. In the present work, neutravidin was favoured over streptavidin for being more specific due to its nearly neutral charge (pI = 6.3)[1].

Neutravidin is a homotetrameric protein with a molecular weight of 60 kDa and an estimated size of about 5 nm in diameter[2]. It has four biotin binding sites, i.e. once it is bound to the membrane lipid, it is still able to bind further biotin. The free binding sites are used to attach a biotinylated Penta-His antibody. Antibodies have a typical molecular weight of about 150 kDa and, considering the Y-shape, they have an approximate overall length of 20 nm.

Kinesin is specifically attached to the Penta-His antibody via its 6xHis-tag ($k_D \leq 10^{-8}$ M), and it is ready to interact with microtubules from the solution. The length of the kinesin construct was calculated to be about 20 nm ([3]).

[1] The pI-value (isoelectric point) is the pH, at which a molecule carries no overall electrical charge.

[2] Assuming that the average density of proteins is $1.38 \cdot 10^3\,\mathrm{kg/m^3}$ [Howard, 2001, p. 29] and 1 Da being $1.66 \cdot 10^{-27}$ kg, the volume of the globular protein can be calculated and the radius for a sphere of that volume can be determined.

[3] For an estimation of the dimensions of the used kinesin construct, the different parts of the truncated construct must be considered: It comprises twice the globular motor domain (350 aa with ellipsoid axes of 7 nm · 4.5 nm · 4.5 nm), the short stalk region (80 aa, corresponding to about 10 nm coiled

3.2 Membrane-Anchored Gliding Assay

Assumptions

Three main assumptions were made for the prediction of the dynamics of a membrane-anchored gliding assay (see also figure 3.2):

(a) The microtubule gliding motion with respect to the substrate is described by the velocity $\vec{v}_{MT}$. It opposes the stepping velocity $\vec{v}_{step}$ of the kinesin on the microtubule reduced by the kinesin velocity $\vec{v}_{kin}$ with respect to the surface (see also figure 3.2a):

$$\vec{v}_{MT} = -\left(\vec{v}_{step} - \vec{v}_{kin}\right) \qquad \text{or} \qquad v_{step} = |-\vec{v}_{kin}| + |\vec{v}_{MT}| = v_{kin} + v_{MT}. \tag{3.1}$$

(b) The stepping velocity of the kinesin on the microtubule $\vec{v}_{step}$ corresponds to the maximum stepping velocity without load, since the stall force of the kinesin is larger than the acting forces in this geometry, which is shown later on in this section.

(c) The system is studied at the equilibrium of forces. This implies that $\vec{v}_{kin}$ and $\vec{v}_{MT}$ are constant, and the overall force disappears. The acting forces are friction forces that arise from the motion in viscous solution and in the membrane. Respectively, and $\vec{F}_{MT}$ is the viscous drag affecting the microtubule and $\vec{F}_{kin}$ names the overall force affecting kinesin motion including the drag from the solution $\vec{F}_{kin}^{solution}$ and from the membrane $\vec{F}_{kin}^{membrane}$. Usually, there will be several motors interacting with one microtubule filament. That means, N motors stepping in an uncorrelated manner on a microtubulus with the same velocity $\vec{v}_{step}$, contribute equally to the friction force of the motors:

$$N \cdot \vec{F}_{kin} + \vec{F}_{MT} = 0. \tag{3.2}$$

coil), the GFP sequence (26 kDa, equals a sphere of 4 nm in diameter) and the short series of the 6x-His.

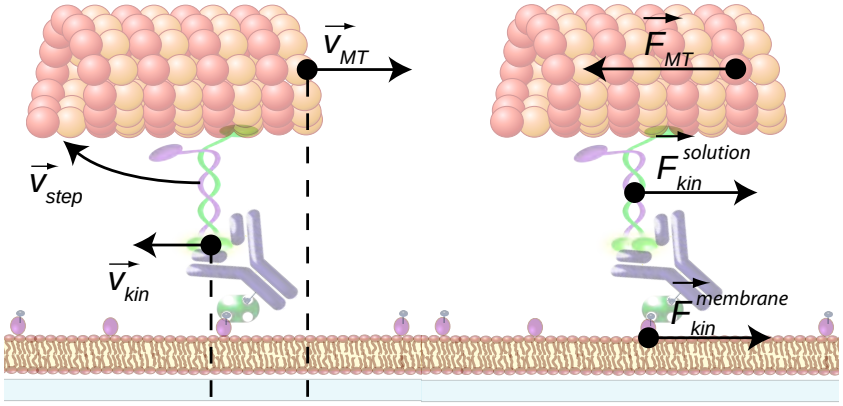

(a) Velocities. **(b)** Forces.

Figure 3.2: Illustration of the vectorial quantities used in the model.

In the following, the maximum friction forces for each component are separately estimated using an upper limit value of v_{step}, i.e. $v_{MT}^{max} = v_{step}$ and $v_{kin}^{max} = v_{step}$ for the two friction forces respectively. Thereby, assumption (b) is confirmed and the magnitudes of the friction forces are demonstrated.

Friction Force Acting on the Microtubule

Gliding of a microtubule through a viscous medium generates a friction force that opposes the driving force, which is applied by the kinesin motors that are attached to the surface. The viscous drag force affecting a microtubule along the central filament axis, $\vec{F}_{MT}$, is given by

$$\vec{F}_{MT} = -\frac{2\pi\eta L}{ln(2h/r_{rod})} \cdot \vec{v}_{MT}, \tag{3.3}$$

using the viscosity of the solution η, the length L of the microtubule, the height h of the filament axis over the surface, the radius of the microtubule r_{rod}, and the gliding velocity $\vec{v}_{MT}$; from [Howard, 2001, p. 107].

The maximum drag force at the highest possible velocity of $v_{MT}^{max} = 1\,\mu\text{m/s}$ follows to be

$$|\vec{F}_{MT}(v_{MT}^{max})| = 70\,\text{fN},$$

for $\eta = 10^{-3}\,\text{Pa·s}$ (water), $L = 20\,\mu\text{m}$, $h = 50\,\text{nm}$ and $r_{rod} = 12.5\,\text{nm}$. The magnitude of

the resultant force confirms the first assumption, because it is almost 100 times smaller than the stall force of a single kinesin (6 pN) and does not affect v_{MT}. For the same reason, v_{MT} does not depend on the number of motors propelling the microtubule in an antibody gliding assay.

Friction Force Acting on the Kinesin

In contrast to microtubules, a kinesin molecule senses two kinds of friction forces: one is caused by the viscous drag of its linker in the solution and the other one is due to the lipid anchor in the SLB. Both forces oppose the direction of motion $\vec{v}_{kin}$, and hence, their values can be added up:

$$\vec{F}_{kin} = \vec{F}_{kin}^{Stokes} + \vec{F}_{kin}^{SLB}. \tag{3.4}$$

The viscous drag in the solution can be roughly estimated using Stokes' law of diffusion for a sphere of radius $r_{sphere} = 20\,\text{nm}$ ([4]) that is pulled through a viscous medium at $v_{kin}^{max} = 1\,\mu\text{m/s}$:

$$\begin{aligned} \vec{F}_{kin}^{Stokes} &= -\,6\pi\,\eta\,r_{sphere}\cdot\vec{v}_{kin} \\ |\vec{F}_{kin}^{Stokes}(v_{kin}^{max})| &= 0.4\,\text{fN}. \end{aligned} \tag{3.5}$$

The drag of the lipid anchor in the SLB can be calculated from the mobility μ of the lipids in the SLB, whereby μ can be substituted by the diffusion coefficient using the Einstein-Smoluchowski-relation, equation (2.3), as follows:

$$\begin{aligned} \vec{F}_{kin}^{SLB} &= -\,\mu_{lipid}\cdot\vec{v}_{kin} \\ &= -\,\frac{k_B T}{D_{lipid}}\cdot\vec{v}_{kin}\,. \end{aligned} \tag{3.6}$$

[4] The kinesin and all the linking components *out* of the SLB have to be considered. The length of the kinesin and of the antibody was used as the radius, although the whole construct is probably not spherical at all (see section 3.1.

Using $k_B = 1.38 \cdot 10^{-23}\,\mathrm{J/K}$, $T = 295\,\mathrm{K}$, and the diffusion coefficient of the lipid in the SLB $D_{lipid} = 5\,\mu\mathrm{m}^2/\mathrm{s}$ (compare Tab. 2.1):

$$|\vec{F}_{kin}^{SLB}(v_{kin}^{max})| = 0.8\,\mathrm{fN}.$$

Hence, the resulting drag force on the kinesin molecule is:

$$\begin{aligned} \vec{F}_{kin} &= \vec{F}_{kin}^{Stokes} + \vec{F}_{kin}^{SLB} \\ &= -\left(6\pi\,\eta\,r_{sphere} + \frac{k_B T}{D_{lipid}}\right) \cdot \vec{v}_{kin} \\ &= -\,\mu_{kin} \cdot \vec{v}_{kin} \\ |\vec{F}_{kin}(v_{kin}^{max})| &= 1.2\,\mathrm{fN}, \end{aligned} \tag{3.7}$$

which is 58-fold smaller than the drag affecting a microtubule gliding at the same velocity. Considering the interaction of several motors with one microtubule, the friction forces can be in the same range and the velocities as well. This means, there is no clear dominance of neither process and the microtubule gliding velocities are expected to be reduced in membrane anchored gliding assays compared to antibody gliding assays.

An Expression for the Microtubule Gliding Velocity

Introducing the recently found expressions (3.3) for the microtubule friction, and (3.7) for the kinesin friction, into the relation of equilibrium forces made in the equation (3.2), yields

$$-N \cdot \left(6\pi\,\eta\,r_{sphere} \cdot + \frac{k_B T}{D_{lipid}}\right) \cdot \vec{v}_{kin} - \frac{2\pi\eta L}{ln(2h/r_{rod})} \cdot \vec{v}_{MT} = 0,$$

and transposing for $\vec{v}_{MT}$:

$$\vec{v}_{MT} = -\;N \cdot \frac{6\pi\,\eta\,r_{sphere} + \frac{k_B T}{D_{lipid}}}{\frac{2\pi\eta L}{ln(2h/r_{rod})}} \cdot \vec{v}_{kin} \tag{3.8}$$

The substitution of $\vec{v}_{kin}$ using equation (3.1) reveals a microtubule gliding velocity that depends on the number of attached kinesin motors N as follows:

$$\vec{v}_{MT} = -\frac{1}{1+\frac{L}{N\cdot\kappa}} \cdot \vec{v}_{step}, \quad \text{whereby} \tag{3.9}$$

$$\kappa = \frac{6\pi\,\eta\,r_{sphere} + \frac{k_B T}{D_{lipid}}}{\frac{2\pi\eta}{ln(2h/r_{rod})}}. \tag{3.10}$$

3.3 Consequences

Kinesin Diffusion at the Membrane

The diffusion coefficient for kinesin and its lipid anchor in the SLB is determined by the Einstein-Smoluchowski-relation, equation (2.3), using the expression of the friction force acting on the kinesin:

$$\begin{aligned} D_{kin} &= \frac{k_B T}{\mu_{kin}} \\ &= \frac{k_B T}{F_{kin}/v_{kin}} \\ &= \left(\frac{6\pi\,\eta\,r_{sphere}}{k_B T} + \frac{1}{D_{lipid}}\right)^{-1}. \end{aligned} \tag{3.11}$$

Note that D_{kin} is independent from v_{kin}, since $F_{kin} \sim v_{kin}$. Using the same values as for equation (3.7) gives

$$\begin{aligned} D_{kin} &\approx 3\,\mu\mathrm{m}^2/\mathrm{s} \\ D_{kin} &\approx \frac{2}{3} \cdot D_{lipid}. \end{aligned}$$

This means that the Stokes diffusion of the kinesin molecule and its linker proteins cause a reduction of D_{lipid} by one third compared to a free lipid diffusing in the SLB (based on $D_{lipid} = 5\,\mu\mathrm{m}^2/\mathrm{s}$).

Microtubule Gliding Velocity

The following conclusions can be drawn from equation (3.9):

(i) At constant motor density at the surface, N will be proportional to the length of the microtubule L. Thus, N and L cancel out in (3.8), i.e. v_{MT} is *independent* from the length of the microtubule L within one experiment.

(ii) However, varying the motor density N/L of kinesin motors interacting with the microtubule changes the microtubule gliding velocity v_{MT}. The relation is presented in figure 3.3 with the shape of the function.

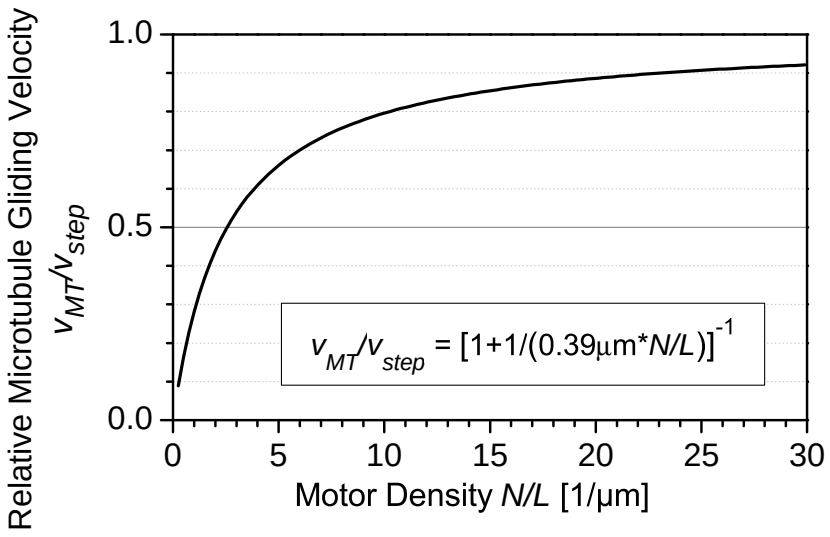

Figure 3.3: Dependency of the relative microtubule velocity v_{MT}/v_{step} from the motor density N/L of kinesin motors interacting with the microtubule, based on equation (3.9), using $\eta = 10^{-3}\,\mathrm{Pa{\cdot}s}$ (water), $r_{sphere} = 20\,\mathrm{nm}$, $k_B = 1.38 \cdot 10^{-23}\,\mathrm{J/K}$, $T = 295\,\mathrm{K}$, $D_{lipid} = 5\,\mu\mathrm{m}^2/\mathrm{s}$, $h = 50\,\mathrm{nm}$, and $r_{rod} = 12.5\,\mathrm{nm}$; $\kappa = 0.39\,\mu\mathrm{m}$ bzw. $\kappa^{-1} = 2.5\,\mu\mathrm{m}^{-1}$.

4 Materials and Methods

This chapter precisely explains how the experiments were practically realized. Therefore, the first section (4.1) contains the names of all the materials used.

In section 4.2, the detailed protocols show how the previously described nanoscopic assemblies of the antibody and the membrane-anchored gliding assay have been produced in flow chambers. The latter has been developed during this work as a composition of (1) vesicle formation and SLB preparation, (2) the incorporation of the SLB into the flow chamber, and (3) the performance of the membrane-anchored gliding assay based on the antibody gliding assay, the latter of which is an established assay in the lab.

Section 4.3 defines the optical instrumentation, the imaging methods applied, and the data processing techniques, including the determination of the lateral diffusion coefficient by Fluorescence Recovery After Photobleaching (FRAP) and by single particle tracking as well as the measuring of microtubule gliding velocities.

4.1 Reagents

Buffers. The used buffers and their compositions are described in table 4.1. All buffers were stored at 5°C.

Lipids. DOPC (1,2-dioleoyl-sn-glycero-3-phosphocholine), mPEG-DOPE (1,2-dioleoyl-sn-glycero-3-phosphoethanolamine-N-[methoxy(polyethylene glycol)2000]) and DSPE-PEG-biotin (1,2-distearoyl-sn-glycero-3-phosphoethanolamine-N-[biotinyl(polyethylene glycol)2000]) were purchased from *Avanti Polar Lipids*. The lipid analogue dye DiD (1,1'-dioctadecyl-3,3,3',3'-tetramethylindodicarbocyanine) was bought from *Invitrogen*. All lipids were stored with argon at −20°C.

Table 4.1: The different buffers used in this study and their compositions.

Buffer	Ingredients
BRB80	80 mM PIPES, 1 mM $MgCl_2$, 1 mM EGTA, KOH to adjust pH 6.9
HEPES	10 mM HEPES, 150 mM NaCl, pH 7.4
PBS	137 mM NaCl, 2.7 mM KCl, 10 mM Na_2HPO_4, 2 mM KH_2PO_4, pH 7.4
TRIS	25 mM Tris-HCl pH 7.5, 150 mM KCl, 5 mM $MgCl_2$

Proteins. Neutravidin from *Pierce* was dissolved to 5 mg/ml and kept at 5°C for up to four weeks. Biotinylated penta-his antibody was bought from *Qiagen* at the original concentration of 200 µg/ml and stored at 5°C as well. Catalase, D-glucose, glucose-oxidase were from *Sigma* and stored at −20°C. The rkin430-GFP plasmid for the truncated GFP-kinesin was kindly provided by R. Cross. It was expressed and purified in house to $c = 280$ µg/ml, and stored at −80°C. Tubulin was extracted from porcine brain, labelled covalently with rhodamine B 1:3, and stored at 4 mg/ml in 5 µl aliquots at −80°C.

Further reagents. PIPES (piperazine-N,N'-bis[2-ethanesulfonic acid]), HEPES (2-[4-[2-hydroxyethyl]-1-piperazinyl]-ethansulfon acid), DMSO (dimethyl sulfoxide anhydrous) and Taxol in DMSO (1 mM) were bought from *Sigma*, $MgCl_2$ was supplied by *Merk*, GTP (guanosine triphosphate) by *Roche*, ATP (adenosine triphosphate) in $MgCl_2$ (100 mM) by *Jena Bioscience GmbH* and DTT (1,4-Dithio-DL-threitol) 1 M in water by *Fermentas*. HEPES and PIPES powders were stored at room temperature, the others at −20°C.

Coverslips. 18 and 22 mm square glass coverslips were from *Corning* and had a thickness of 170 µm. For different applications they had been treated with different techniques to gain certain surface conditions as follows: (i) The easyclean coverslips were washed in mucasol (1:20) solution under sonication and ethanol wash. (ii) Dichlorodimethylsilane (DDS) coated coverslips are hydrophobic, silanised coverslips that facilitate protein adhesion. (iii) PEGylated coverslips were produced by piranha etching and subsequent silanization with PEG (poly[ethylene glycol]), for the purpose that the PEG chains at the surface suppress protein adhesion to the surface. Plasma cleaning was done with easyclened coverslips using 60% RF-power under constant oxygen flow at 0.3 mbar for 1 min.

Fluorescent Dyes. Several components comprised different fluorescent dyes for visualisation. Table 4.2 summarises the used dyes with their fluorescence properties. The

according filtersets used for imaging can be taken from table 4.3 of section 4.3. The values were taken from http://info.med.yale.edu/genetics/ward/tavi/FISHdyes2.html (last checked Feb 16, 2010).

4.2 Protocols

Antibody Gliding Assay

Flow chamber. A flow chamber like the one shown in figure 4.1a was used for sequentially introducing the proteins into the flow chamber. Its basis was a 22 mm square DDS coverslip. Several stripes of scotch tape of 2 mm width were attached to the DDS-coated glass at 1-2 mm distance. The flow chamber was closed by a second, 18 mm square coverslip with a PEGylated surface creating two to four separate flow channels of about 5 µl volume.

Microtubule polymerisation. Microtubules self-assemble from tubulin protein under appropriate conditions. Therefore, 1.5 µl of the polymerization mix, which comprised of 1.2 µl pure DMSO, 1 µl $MgCl_2$ ($c = 100\,\mathrm{mM}$), 1 µl GTP ($c = 25\,\mathrm{mM}$) and 1.8 µl BRB80, were added to 5 µl tubulin ($c = 4\,\mathrm{mg/ml}$). The tubulin-polymerization mix was vortexed and incubated in a heat block for at least 30 min. To stop the polymerization process, 500 µl BRB80-taxol (BRB80 buffer containing 10 µM taxol) were added and the mix was vortexed shortly. Then, the solution was centrifugated for 5 min in a *Beckman* air centrifuge[1] leaving a pellet of microtubules at the ground of the tube. To get rid

[1] Used with the black rotor, $f_g = 1.12 \cdot 17.6\,\mathrm{mm} \cdot (85\,\mathrm{rpm})^2 = 142.4 \cdot g$.

Table 4.2: Fluorescence properties of the used dyes related to the labelled components, characterised by the wavelengths of the absorption and emission peaks (color of light in brackets).

Dye	Component	Absorption [nm]	Emission [nm]
rhodamine B	microtubules	540 (green)	625 (red)
GFP	kinesin	498 (blue)	516 (green)
DiD	membrane	644 (red)	665 (far-red)

of unbound tubulin, the supernatant was discarded and the pellet was resuspended in 200 µl BRB80-taxol. The resulting solution is referred to as MT200.

Flow sequence. The flow chambers were filled with buffer (BRB80 or PBS) with the help of low pressure flow. Afterwards, the first component to be added was the anti-His antibody (20 x diluted to $c = 31$ nM), which unspecifically attached to the surface during 5 min incubation time. Then, the sample was rinsed with the same buffer and incubated with F127 surface blocking polymer (1 % in the respective buffer) for another 5 min, to prevent further protein adhesion at the surface. Next, the kinesin solution ($c = 280$ µg/ml His-GFP-rk430: $100 \ldots 10,000$ x diluted, 1 mM ATP) was introduced into the flow chamber. After 5 min it was washed out with motility solution containing 1 mM ATP, 18 mM D-Glucose, glucose-oxidase ($c = 25$ µg/ml), catalase ($c = 10$ µg/ml), 5 mM DTT, 10% MT200 (microtubules in BRB80-taxol) and 10 µM Taxol.

Membrane-Anchored Gliding Assay

Flow chamber. The two types of flow chambers that have been used during this study are presented in figure 4.1. The pure *glass flow chamber* (see figure 4.1a) was similar to the flow chamber described for the antibody gliding assay but the basal DDS coverslip was substituted by easycleaned glass that had been freshly plasma cleaned immediately before usage. This treatment generated a strongly hydrophilic surface that allowed for SLB formation similarly well than on a mica surface (see also section 2.2. A *mica flow chamber* (figure 4.1b) was based on a 22 mm square easycleaned glass coverslip. A small droplet of immersion oil was deposited on top of the glass, followed by an thin slice of freshly cleaved mica. Then, several stripes of scotch tape were attached to the mica surface at 1-2 mm distance and covered by one half of an 18 mm PEG coverslip forming channels of about 3 µl volume.

The preparation of a SLB in the flow chamber required several steps that are schematically illustrated in figure 4.2 (see below).

Vesicle formation from lipids. The desired composition of lipids in chloroform was mixed in a glass vial to 100 µl with a final concentration of 10 mg/ml. The used lipid mix mainly consisted of DOPC and was labelled with $0.1 - 0.2$ mol% DiD. Furthermore,

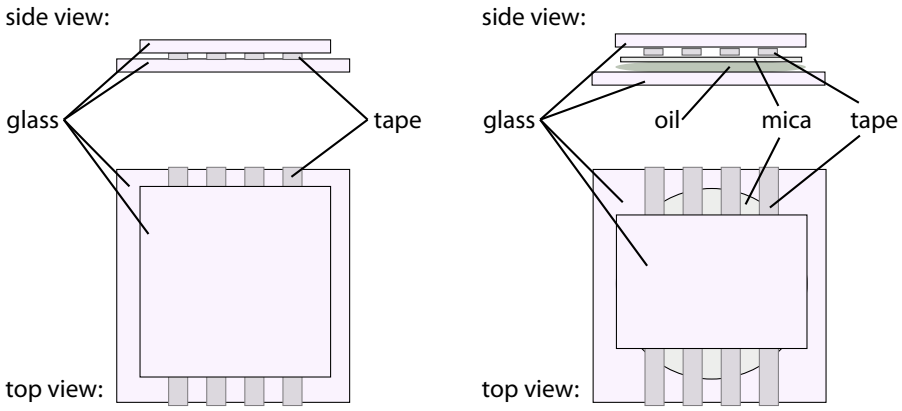

(a) Glass flow chamber. **(b)** Mica flow chamber.

Figure 4.1: Two types of flow chambers made of glass coverslips glued with scotch tape that also formed the several channels, (a) pure glass coverslip, and (b) with and additional mica sheet.

it contained $0.01 - 1\,\text{mol}\%$ DSPE-PEG-biotin for functionalisation, plus, in some cases additional mPEG-DOPE to a final fraction of $5\,\text{mol}\%$. The lipid mixture was dried under nitrogen flow so that the lipid material was deposited at the walls of the vial. The vial was completely dried in a vacuum chamber (30 min). The lipids were rehydrated in $100\,\mu\text{l}$ of the buffer solution (TRIS, PBS or HEPES) and vortexed for about 1 min to dissolve the lipid residues in the vial. The solution was left to equilibrate at room temperature for another 20 min and subsequently vortexed again. The resulting solution comprised multilamellar vesicles (MLVs) of about $1\,\mu\text{m}$ size that strongly scatter the daylight reasoning the milky appearance of the solution as depicted in figure 4.3. At that state vesicles were frozen in $10\,\mu\text{l}$ aliquots at $-20°\text{C}$.

Generation of SUVs from MLVs. For SLB formation small unilamellar vesicles (SUVs) are needed. Therefore, $10\,\mu\text{l}$ of the MLV solution were diluted in $150\,\mu\text{l}$ of the appropriate buffer and sonicated in an ultrasonic bath until the solution had become clear. That means the MLVs had been disrupted and had formed SUVs, which are too small to scatter light.

SLB formation in the flow chamber. After the flow chamber was prepared with either of the described methods, $19\,\mu\text{l}$ of the SUV solution were mixed with $1\,\mu\text{l}$ of $CaCl_2$

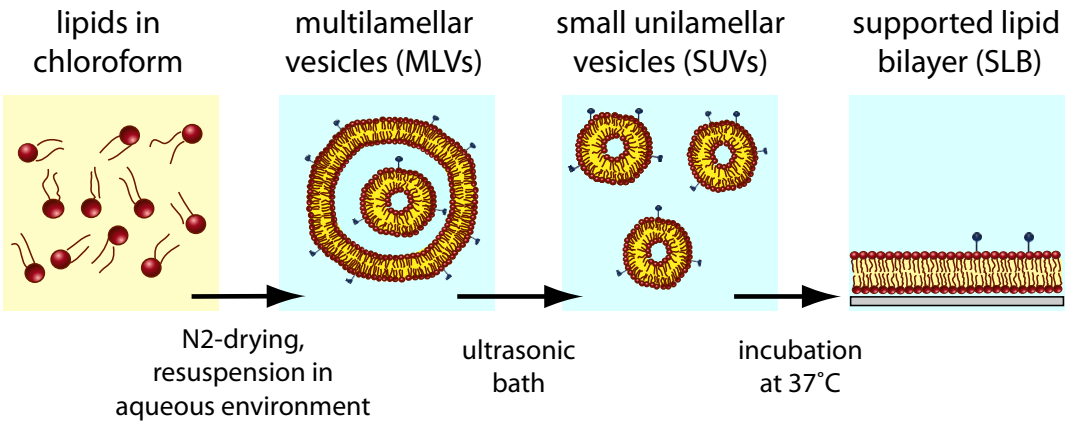

Figure 4.2: Scheme of the making of a SLB from lipids dissolved in chloroform. In the first step the lipid mix is completely dried and rediluted in aqueous buffer solution, sonication of the MLVs makes them smaller (SUVs) and incubation on a hydrophilic surface allows vesicle formation by adhesion and subsequent rupture of the SUVs.

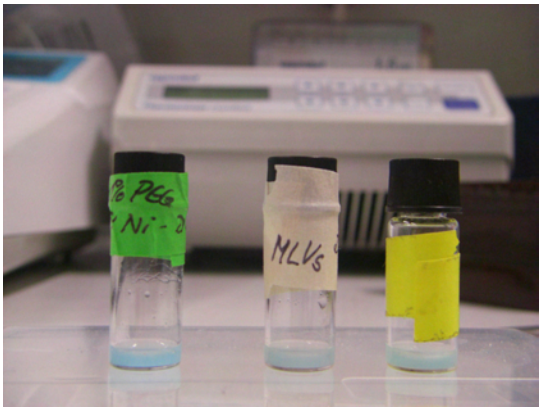

Figure 4.3: Picture of the different lipid compositions of MVLs before aliquoting and freezing.

1 M and immediately poured into each channel of the flow chamber. Thereby, the Ca^{2+}-ions destabilised the vesicles and induced vesicle rupture. The whole flow chamber is placed into a small plastic box, covered with a sheet of wet filter paper (to reduce evaporation) and incubated for 30 min at 37°C. The bilayer formation was completed by washing with 100 µl of warm (37°C) buffer solution.

Kinesin binding and gliding assay. In the next step, the kinesin linking proteins were sequentially flown through the channels of the flow chamber. The necessary amounts of the proteins had been estimated and the concentrations appropriately adjusted. The following flow sequence was introduced at room temperature:

- 10 µl neutravidin ($c = 5$ µg/ml), 5 min incubation
- 60 µl buffer wash
- 10 µl biotinylated penta-his antibody ($c = 10$ µg/ml)[2], 5 min incubation
- 20 µl buffer wash
- 10 µl kinesin solution ($c = 280$ µg/ml His-GFP-rk430: 10 x . . . 1,000,000 x diluted, 1 mM ATP), 5 min incubation
- 10 µl antifade/motility solution, containing 1 mM ATP, 18 mM D-Glucose, glucose-oxidase ($c = 25$ µg/ml), catalase ($c = 10$ µg/ml), 5 mM DTT, ± 10% MT200 (microtubules in BRB80-taxol) and 10 µM Taxol, 5 min incubation (before imaging)

4.3 Optical Setup and Imaging

Fluorescent Imaging System

Fluorescent imaging was performed at room temperature using two optical setups of a *Zeiss Axiovert 200 M* inverted fluorescence microscope in combination with the filtersets presented in table 4.3. The first setup used was an *epi-fluorescence* microscope with a *Plan Neofluar 100x Oil* objective having a numerical aperture of 1.3 and a working

[2] That is 50-fold lower than in the antibody gliding assay but it corresponds to the number of neutravidin molecules attached to the SLB.

distance of 170 µm. Images were acquired using a back-illuminated *Micromax* camera with a 512 x 512 pixels CCD-chip of 13 µm pixel size and the illumination light came from a *lumen 200* mercury-lamp.

Table 4.3: Filtersets used with nm-wavelength of their bandpass (centre/width) and longpass filters related to the component they were imaging.

Filterset	Excitation	Dichroic	Emission	Component
TRITC	535/50	565	610/75	microtubules, (membrane)
FITC	480/40	505	535/50	kinesin (epi)
laser GFP	488/10	505	515/30	kinesin (TIRF)
Cy5	630/40	660	690/40	membranes

The second setup for TIRF microscopy was equally equipped, but it furthermore comprised a TIRF slider (*Zeiss*) and a laser input for GFP-kinesin excitation (*Innova 70C Spectrum* applied at 488 nm with a power of about 32 mW). Here, the used objective was an *α-Plan-Apochromat 100x Oil* with a numerical aperture of 1.46. In the TIRF setup, image acquisition was realised by an *Andor iXon plus* camera with 512 x 512 pixels exhibiting a square size of 16 µm.

During this study image acquisition and processing was done using *Metamorph* software from *Universal Imaging*. For fitting of the experimental datasets, *OriginLab 7.0* was employed. Large data collections and calculations were handled with *Microsoft Excel*.

Diffusion Measurements Using FRAP

The *fluorescence recovery after photobleaching* (FRAP) method as described by [Axelrod et al., 1976] was applied for characterisation of lipid diffusion in a SLB. The main idea of that work is to bleach a specific region of the labelled membrane with a powerful laser beam and measure the fluorescence recovery due to lateral diffusion of bleached and unbleached molecules in the membrane. The characteristic recovery time τ_D characterises the two-dimensional diffusion of the lipids in the membrane.

In the present work, bleaching was realised by an arc lamp in combination with an aperture diaphragm such that a circle region of the sample was continuously illuminated

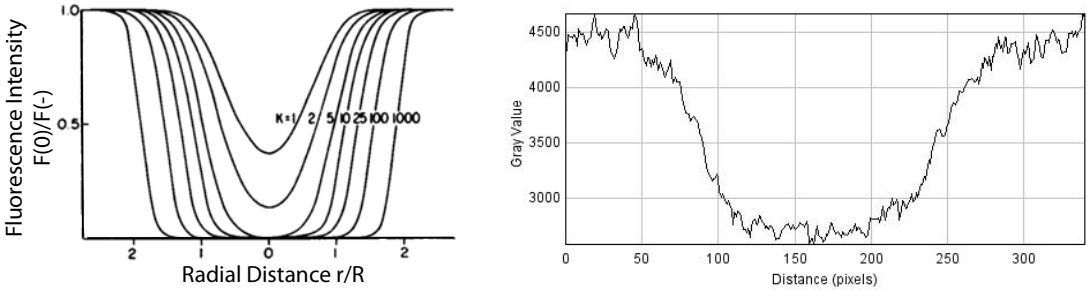

(a) Theory. **(b)** Experiment.

Figure 4.4: Post-bleach fluorescence intensity before fluorescence recovery, (a) theoretically, with a GAUSSian beam of radius R at e^{-2} intensity for various values of the bleaching parameter K, adapted from [Axelrod et al., 1976], and (b) from the experiment at $R = 10.4\,\mu\text{m} \mathrel{\hat{=}} 80\,\text{pixels}$.

for 30 s ([3]). Immediately after bleaching, the fluorescence was recorded at closed aperture in image stacks comprising an image series, which was obtained using an illumination time of 100 ms per frame and constant time intervals between two images Δt_{frap} from 1 s to 20 s. For data evaluation, the average fluorescence intensity of the circle region was plotted over time for each image of the stack. The plot demonstrates the recovery process (see also figure **??**), which was analysed as follows.

In [Axelrod et al., 1976], the time dependant solution of the theoretical fluorescence intensity recovery is derived from FICK's laws of diffusion. Thereby, the initial fluorescence after bleaching $F(0)$ depends on the illumination beam profile that has been differentiated to be either GAUSSian as presented in figure 4.4a, or a uniform circular disc profile. Although in the present study bleaching was accomplished by a circular aperture at wide-field illumination that is constant over the bleached region, the recorded fluorescence intensity profile at $t = 0$ was not a uniform circular disc but a GAUSSian beam profile (compare figure 4.4b). This appearance might be explained by the long illumination times necessary to bleach the fluorophores with the lamp. According to [Axelrod et al., 1976], the average fluorescence intensity directly after bleaching, $F(0)$, is characterised by the fluorescence intensity before bleaching, $F(-)$, and the initial parameter

[3] In contrast, the necessary illumination time with a laser would be in the range of only a few seconds.

K for a GAUSSian beam profile:

$$F_K(0) = F(-) \cdot \frac{1 - e^{-K}}{K}. \tag{4.1}$$

In the named publication it was obtained that the fluorescence intensity recovery, $F_K(t)$, is best described by

$$F_K(t) = F(-) \cdot \sum_{n=0}^{\infty} \frac{(-K)^n}{n! \cdot [1 + n(1 + 2t/\tau_D)]}. \tag{4.2}$$

That means $F_K(t)$ is completely determined by the characteristic recovery time τ_D and K. For fitting the experimental dataset $F(-)$ was substituted by $F_K(\infty)$ to account for incomplete recovery due to bleaching of fluorescence from immobile objects at the surface. Furthermore, the infinite sum was approximated by $n = 0...8$ leading to the final fit function

$$F_K(t) = F_K(\infty) \cdot \sum_{n=0}^{8} \frac{(-K)^n}{n! \cdot [1 + n(1 + 2t/\tau_D)]} \tag{4.3}$$

with the three fit parameters $F_K(\infty)$, K and τ_D.

The fraction of mobile fluorophores can be calculated from

$$M = \frac{F_K(\infty) - F_K(0)}{F_K(-) - F_K(0)}, \tag{4.4}$$

and according to [Axelrod et al., 1976] the diffusion constant D is related to τ_D via

$$D = \frac{R^2}{4\tau_D}. \tag{4.5}$$

The knowledge of D_{lipid} allowed the comparison of the SLB formation method applied during this work to the experimental diffusion coefficients obtained by others (table 2.1). On the other hand, the FRAP method was also used to study the D_{kin} of the kinesin diffusion on top of the SLB, which was identified to influence the microtubule gliding velocity in the membrane-anchored assay (chapter 3). Alternatively, D_{kin} was determined from the mean square displacement of single molecule trajectories of the GFP-kinesin.

Kinesin Single Molecule Imaging and Tracking

Since fluorescent dyes photobleach after a certain time, the lifetime of a fluorophore limited the total imaging time for GFP-kinesin to about 10 s in the used setup. For the observation of fast single molecule movements such as the diffusion of kinesin molecules anchored to the SLB, continuous image stacks or *streams* were recorded with an illumination time of 100 ms per frame[4].

For high precision reconstruction of the trajectory of the molecules, a tracking software written in-house was used (*Fiesta*, see also [Nitzsche et al., 2008]). The software fits the single molecule intensity spot with a two-dimensional GAUSSian function and detects the positions of the molecule from the centre of the spot for each frame with nanometre precision. Subsequently, the position measurements were connected to rebuild the trajectories of single molecules.

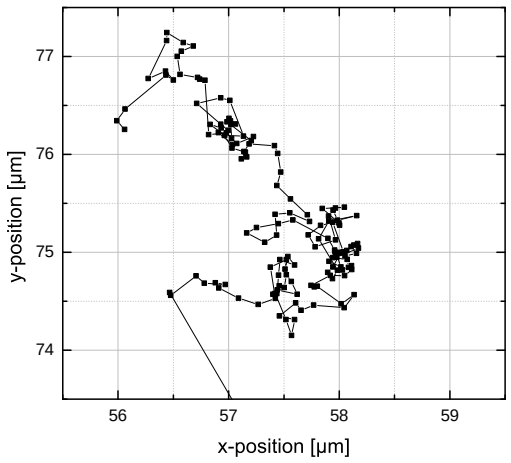

Figure 4.5: Example of the trace of a molecule obtained by Fiesta tracking software.

The tracks of the diffusing kinesin molecules have been used to calculate the mean square displacement for individual molecules as well as for the whole population. Thereby, different time intervals Δt_{spt} have been evaluated such that the displacement between

[4]The camera chip was illuminated for 100 ms and the illumination period is followed by a short readout time of about 35 ms. Thus, it takes 135 ms to record one frame.

two images of 2, 4, 8, 16, 64 and 128 frames were generated, without overlapping of the pooled time intervals. According to equation 2.2a derived in section 2.2, the diffusion coefficient was determined from the slope of a linear fit to a $\langle \Delta x^2 \rangle$ versus Δt_{spt} plot, weighted by the number of detected intervals.

The bleaching effect in continuously illuminated stream stacks can also be employed to confirm the observation of single molecules. Since the kinesin is dimeric, a functional GFP-kinesin molecule is expected to bleach in two steps, because the two GFP molecules bleach independently from each other. Figure 4.6 exemplarily shows the fluorescent intensity of a kinesin molecule decreasing to background level in two distinguishable steps proofing the observation of single GFP-kinesin dimers rather than protein clusters. Generally, this analysis would have to be carried out for each molecule individually, which is not always possible. This criterion was applied to several molecules per stack and only spots of comparable intensity were included into the data evaluation.

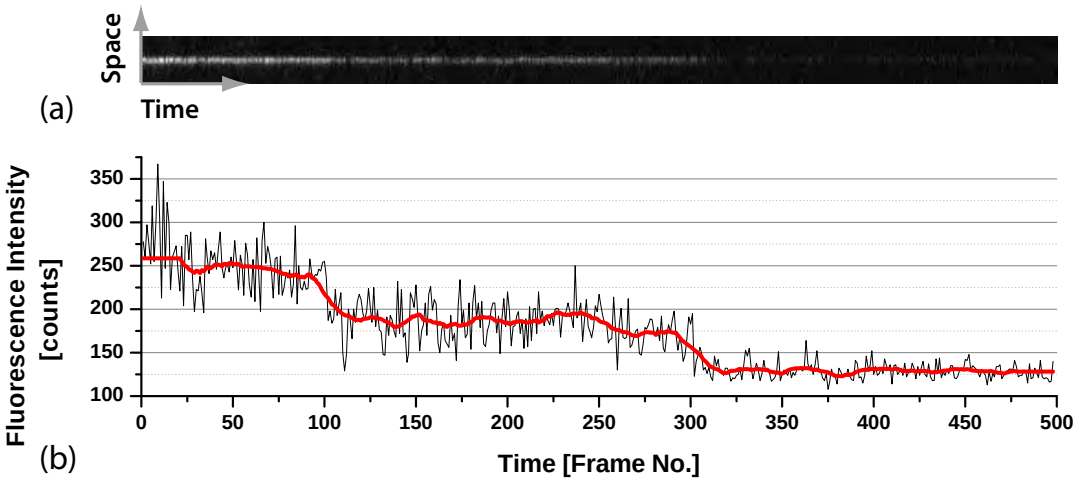

Figure 4.6: Two-step bleaching proof of single molecule detection: (a) fluorescent intensity kymograph (intensity image of a pixel row over time), and (b) fluorescent intensity evolution (profile of the central line in the kymograph) in counts with the two clearly separated bleaching steps, whereby the final level of 130 counts equals the noise level, 1 frame $\hat{=}$ 0.1 s.

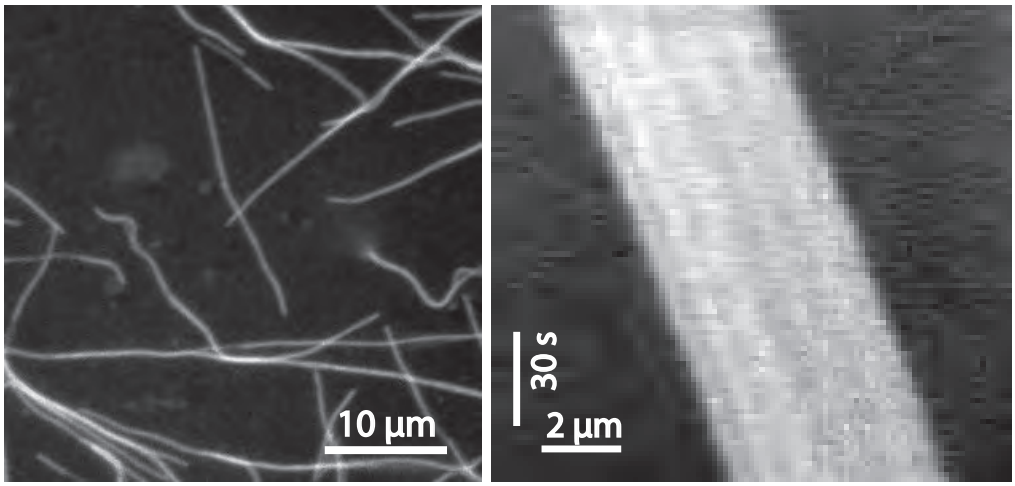

(a) Maximum projection. **(b)** Kymograph.

Figure 4.7: Microtubule motion observed in fluorescence intensity image stacks: (a) maximum projection of the the fluorescent intensity per pixel of the images of one stack, allows for definition of the microtubule gliding trajectories, (b) intensity along the central filament line of a microtubule trajectory (horizontal axis) versus time (vertical axis) in a kymograph image.

Imaging and Evaluation of Microtubule Motility

Microtubule motility was recorded in *time lapse* stacks that consist of instantaneous frames with fixed time intervals in between. Typically, time intervals of 1 to 2 s have been used for microtubule imaging, whereby each frame was illuminated for 100 ms.

The trajectory of the microtubule motion was gained from the maximum projection as shown in figure 4.7a by manual tracking. The fluorescence intensity along the trajectory of the central filament line was extracted to a distance versus time plot or *kymograph* image (figure 4.7b). The slope of the tip was used to determine the average gliding velocity of the microtubule.

5 Results and Discussion

This chapter is divided into the different steps of the experiment. It starts with a summary of the expertise that has been gained during the development of a protocol for the successful formation of supported lipid bilayers (SLBs) in the flowcell (section 5.1). Furthermore, bilayer imaging using the fluorescence recovery after photobleaching (FRAP) method (described in section 4.3) is analysed and the diffusion constant D_{lipid} is calculated from the experimental data.

Subsequently, the diffusion constant of kinesin anchored to an SLB, D_{kin}, was determined and compared with the diffusion of the lipid dyes D_{lipid} (section 5.2). The measurement of D_{kin} allows for the direct determination of the mobility of the kinesin molecules, which is related to the friction force facilitating microtubule motility (see also section 3.2). For different motor densities in the SLB, two methods have been applied: FRAP was used for high kinesin densities at the surface and single particle tracking enabled investigation of very low amounts of kinesin bound to the SLB.

In the last paragraph, 5.3, microtubule gliding on SLBs is demonstrated. The obtained microtubule velocities for the membrane-anchored gliding assay are related to the control (antibody gliding assay), and the experimental findings are compared to the model that has been developed in chapter 3.

5.1 Generation of Supported Lipid Bilayers and Lipid Diffusion

Aspects of Bilayer Formation in the Flowcell

SLBs have been prepared as described in section 4.2. While processing the protocol, the following issues have been worked out to be especially important.

Buffer usage. In HEPES, TRIS and PBS (see table 4.1), SLBs were found to form well. However, the TRIS buffer used in [Loose et al., 2008] led to complications when deep-freezing the lipid vesicles for storage. Furthermore, only HEPES and PBS were supposed to be appropriate as a kinesin buffer that keeps the protein stable, and they were therefore favoured over TRIS. The HEPES buffer has not been extensively tested in conjunction with motor proteins, but it seemed to hinder the kinesin diffusion on top of the SLB. In PBS, kinesin diffusion and microtubule motility was observed, and therefore, most of the presented results have been obtained in PBS buffer. Generally, after successful formation of the SLB, buffer exchanges (e.g. to BRB80 or even water) did not influence the stability of the SLB.

$CaCl_2$ concentration. For the different buffers, the amounts of Ca^{2+}-ions necessary for vesicle rupture were discovered to vary. The experiments in HEPES buffer worked out at 3 mM $CaCl_2$. In PBS, SLBs formed nicely for concentrations from 25 mM to 100 mM, although they seemed to be less stable at lower concentrations. Without Ca^{2+} ions, only undesired vesicular structures could be observed at the surface. Consequently, 50 mM $CaCl_2$ have been used (as described in the protocol in section 4.2).

Vesicle size. The small size of the SUVs was essential for a successful SLB formation. Therefore, the sonication procedure is the determining step. Only if the solution had become clear (i.e. vesicles are too small to scatter light), the vesicles formed a smooth bilayer in the flowcell, whereas the time in the ultrasonic bath could not be utilised as a criterion for SUV formation. Using elder vesicles (not freshly defrosted or already stored for more than two months) was problematic: Over long time scales, the MLVs might fuse for energy minimisation and apparently could not become SUVs from sonication as easy as before. Utilising a non-homogeneous vesicle solution resulted in an inhomogeneous

bilayer with lots of bigger vesicles and tubes on the surface.

Hydrophilicity of the surface. Only strongly hydrophilic and negatively charged surfaces, such as a freshly cleaved mica sheet or a plasma cleaned glass surface, allowed for vesicle adhesion and subsequent vesicle rupture. In contrast, easycleaned and PEGylated glass surfaces were found to be *not* applicable for bilayer formation, in spite of their hydrophilicity.

Lipid composition. Since all the used lipid compositions mainly contained DOPC, there has not been much variation, and all of them allowed nice bilayer formation. For vesicles comprising 5 mol% PEG-lipids, small non-fluorescent areas of $\sim 1\,\mu$m diameter were observed after washing with room temperature buffer. The dark spots were equally distributed in the SLB. Subsequent kinesin linkage led to accumulation at the spots. Therefore, the spots have been identified to be either holes in the SLB, which were possibly caused by the high ratio of PEGylated lipids with the big PEG pellet on top of them, or a phase separation effect due to equilibrium sorting at this certain lipid composition. The data presented in the following was generated using SLBs with 1 mol% PEG-lipids and less, that did *not* show visible phase separation.

Diffusion Coefficient of the SLB Obtained by FRAP

Following the FRAP imaging procedure described in the methods part (chapter 4), figure 5.1a visualises the appearance of an SLB on a glass surface before ($t = -30\,$s) and after bleaching ($t = 0\,$s) at closed aperture. Until $t = 0\,$s, the fluorescence has decayed due to the continuous illumination. In the following three images, the intensity is rising again, which is further clarified by the intensity plot in figure 5.1b. Altogether, the mobility of the fluorescent lipids was verified, confirming the existence of an SLB.

Figure 5.1b demonstrates that the fluorescence recovery data can be well described using the fit function (4.3),

$$F_K(t) = F_K(\infty) \cdot \sum_{n=0}^{8} \frac{(-K)^n}{n! \cdot [1 + n(1 + 2t/\tau_D)]},$$

which has been motivated in section 4.3. From the resulting fit parameters K, τ_D, and

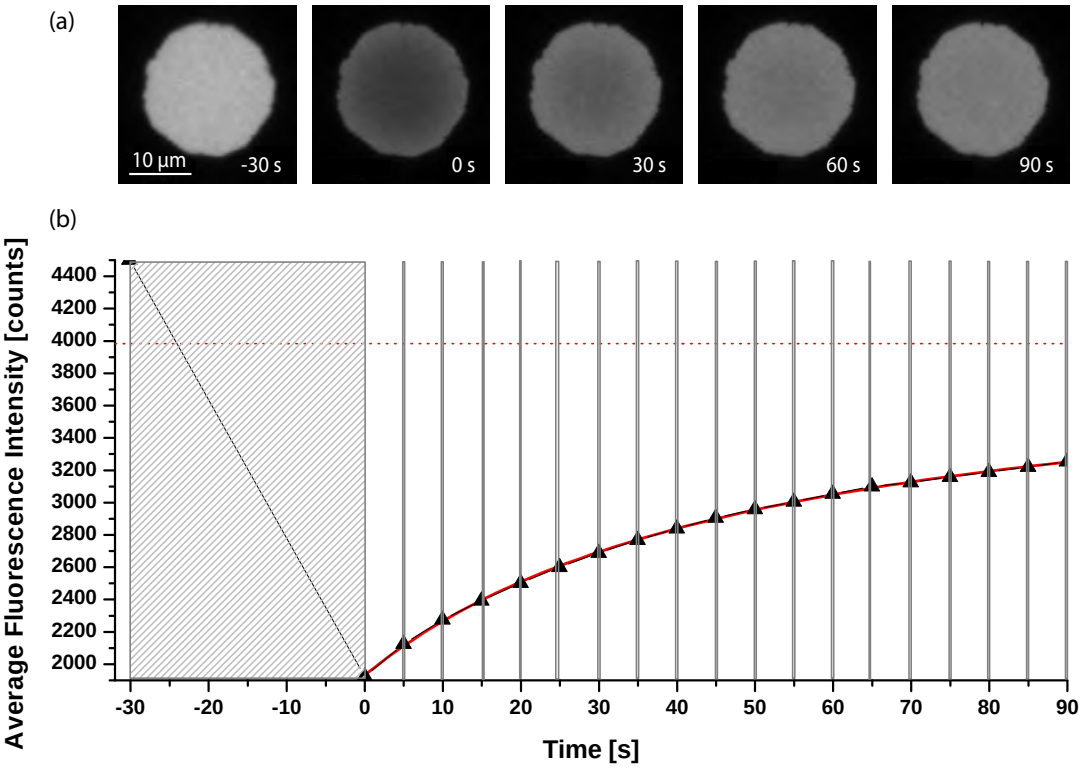

Figure 5.1: Measuring fluorescence intensity recovery of an SLB in PBS: (a) selected timelapse images in the Cy5 filter channel before ($t = -30\,\mathrm{s}$) and after bleaching, labelled with the imaging time in s ($t = 0\,\mathrm{s}$ denotes the start of recovery imaging), equally scaled; and (b) fluorescence intensity plot (averaged over the spot) over time of the timelapse stack shown in (a), vertical grey areas indicate sample illumination, the red curve is the fit function to the data and the dashed line marks the asymptote from the fit, $F_K(\infty) = 3992 \pm 10$, further fit values are $\tau_D = 46.6 \pm 0.8\,\mathrm{s}$ and $K = 2.00 \pm 0.02$.

$F_K(\infty)$, the SLB can be characterised as follows:

- For all experiments, the bleaching parameter K was about 1.5, according to the fact that the theoretical bleaching intensity profile for $K = 1$ in figure 4.4a compares to the experimental one in figure 4.4b. The similarity of the K values is a confirmation of the bleaching process being constant during the different experiments. Due to the theory, K is a measure for the bleaching process and does not say anything about the recovery process.

- The asymptote $F_K(\infty)$ varied in the range of several thousand counts. The fluctuations can be explained by varying initial conditions between different experiments. However, information can be gained from the mobile fraction M, which is defined by $F_K(\infty)$ via equation (4.4). The calculated M values were between 75 and 90 %. They can be seen as an indicator of homogeneity of bilayer formation. Furthermore, $F_K(\infty)$ was lowered by unwanted bleaching during image acquisition in the recovery phase, which makes M appear small (see also equation (4.4)). In the corresponding time lapse images, only few immobile particles have been observed.

- The fit value of the characteristic recovery time τ_D ranged from 30 to 80 s. Depending on the radius of the bleaching spot R, equation (4.5) yielded diffusion constants $D_{lipid} = (0.593 \pm 0.012)\ \mu m^2/s$. This value is about 10-fold less than expected from table 2.1 for lipid diffusion in SLBs. Therefore D_{lipid} has been investigated in further detail.

Figure 5.2 illustrates the influence of the imaging interval Δt_{frap} on the diffusion coefficient D_{lipid}. For one SLB, D_{lipid} did not vary to much when using different imaging intervals $\Delta t_{frap} = 1...20\,s$ between two images. This can be seen from the fit curves to the recovery data in figure 5.2a. Furthermore, figure 5.2b) shows the corresponding K-values for the different imaging intervals, whereby, $K(\Delta t_{frap} = 1s)$ is considerably different from K for the longer imaging intervals. However, since K is only determined by the bleaching, it should be constant for all recovery curves originating from one and the same bilayer. Thus, the recovery curves obtained using $\Delta t_{frap} = 1s$ are *not* described well by the theory (probably because of unwanted bleaching while illuminating the sample for fluorescence recovery imaging). Therefore, they were obtained to be inappropriate for the data evaluation of fluorescence recovery. Neither were the 20 s intervals, because imaging would either take very long or generate only few data points for fitting.

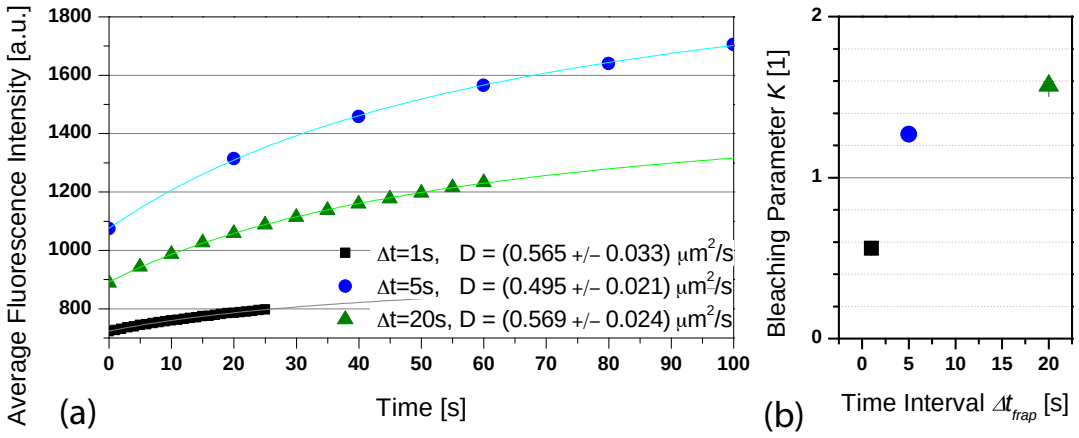

Figure 5.2: Influence of imaging interval Δt_{frap} on the calculated diffusion coefficient D_{lipid}: (a) fluorescence recovery curves for different imaging intervals Δt_{frap} of one and the same bilayer with their calculated diffusion coefficients D_{lipid} from the corresponding fit, and (b) diffusion coefficient D_{lipid} and bleaching parameter K replotted versus Δt_{frap}.

That is why $\Delta t_{frap} = 5\,\mathrm{s}$ was used for fluorescence recovery imaging.

It was noted that the binding of kinesin to the SLB did *not* influence the diffusion of the DiD[1] lipid dye in the SLB. D_{lipid} and M from SLBs with kinesin attached integrate into the population of the DiD diffusion without the kinesin attached (see also figure 5.5).

To investigate the deviation of D_{lipid} from the literature, the measurements were repeated with laser bleaching using a laser scanning microscope[2]. The recovery of fluorescence intensity was equally recorded and evaluated, resulting in about two-fold higher diffusion constants (data not shown).

On the other hand, D_{lipid} was found to be increased by a factor of 2 when using the mica support instead of the plasma cleaned glass (figure 5.3).

[1] 1,1'-dioctadecyl-3,3,3',3'-tetramethylindodicarbocyanine, see also section 2.3 or 4.1.
[2] The device used was an inverted *Zeiss LSM 405/594* and a laser emitting at 633 nm.

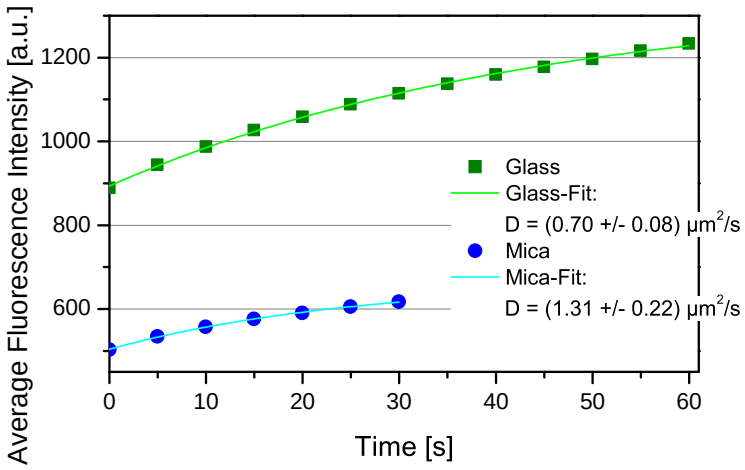

Figure 5.3: Recovering fluorescence intensity (averaged over the bleaching spot) of SLBs prepared on mica and plasma cleaned glass support (symbols), fitted by (4.3) (lines), whereby the same SUVs were used for SLB formation.

Discussion

The determined diffusion coefficients have been found to be very reproducibly $D_{lipid} = (0.59 \pm 0.19)\ \mu m^2/s$. This value is about 10-fold smaller than D_{lipid} found in the literature for SLBs with similar lipid compositions. However, D_{lipid} was found to vary for different supports, and it is also known to be very sensitive to the SLB formation methods [Seu et al., 2007, Scomparin et al., 2008]. Due to the many steps, the preparation procedures of the different references are hardly comparable, neither among each other nor to the experiments of this work. A variance of a factor of two can also be attributed to the error committed by the simplified bleaching method with the subsequent FRAP data evaluation of the SLBs bleached with an arc lamp instead of a laser (see also section 4.3). Therefore, the discrepancy of a factor of 10 was deemed acceptable.

In spite of the determined diffusion constants being smaller than in the literature, homogeneous SLBs were produced and the intensity recovery was clearly detectable.

5.2 Diffusion of Membrane-Anchored Kinesin

Kinesin Diffusion Coefficient Obtained by FRAP

After sequentially flushing the binding components through the flowcell using a high concentration of GFP-kinesin in the solution (100 x diluted, $c_{final} = 2.8\,\mu g/ml$), the fluorescence of kinesin molecules was observed with the FRAP method. The imaging was done analogically to the DiD diffusion in the SLB, but using the FITC filter for recording of the GFP-signal (instead of Cy5 for DiD). For the kinesin FRAP measurements, the antifade solution was substituted by an ATP-containing buffer. This avoids the diffusive fluorescence intensity recovery to be superimposed by chemical fluorescence recovery from off-state molecules, which has been observed when using the oxygen scavenger system (data not shown). The chemical recovery was especially obvious during the first seconds after bleaching.

Figure 5.4 exemplarily shows the data of the fluorescence recovery of GFP-kinesin attached to an SLB, which contained 1 mol% DSPE-PEG-biotin, for different imaging intervals Δt_{frap}. In spite of the high concentrations of kinesin on the surface, the fluorescence intensity was very low compared to the fluorescence of the lipid dye. To improve the informative value for the low fluorescence signal of the GFP-kinesin, the background noise had been subtracted in this case. The low number of photons was attributed to the GFP being a completely different molecule than the lipid dye, that tends to bleach very quickly without the oxygen scavenger system in the solution.

The data for $\Delta t_{frap} = 5\,s$ shows an initial fluorescence increase after bleaching, that is getting overwhelmed after a certain time by another effect, which is interpreted as bleaching caused by imaging in a manner such that bleaching was faster than fluorescence recovery. Elongating the imaging interval to $\Delta t_{frap} = 60\,s$ (red symbols in figure 5.4) resolved the problem so as to enable curve fitting and subsequent determination of $D_{kin} = (0.065 \pm 0.009)\ \mu m^2/s$. However, imaging over time scales that long, it is challenging to keep the imaging conditions constant (e.g. holding the sample in focus).

In figure 5.5, the diffusion coefficients determined by several FRAP measurements of the GFP- and DiD-signal are plotted versus the appropriate mobile fraction M, which is defined by $F_K(\infty)$ (from the fit) via (4.4). The diagram shows a group of diffusion

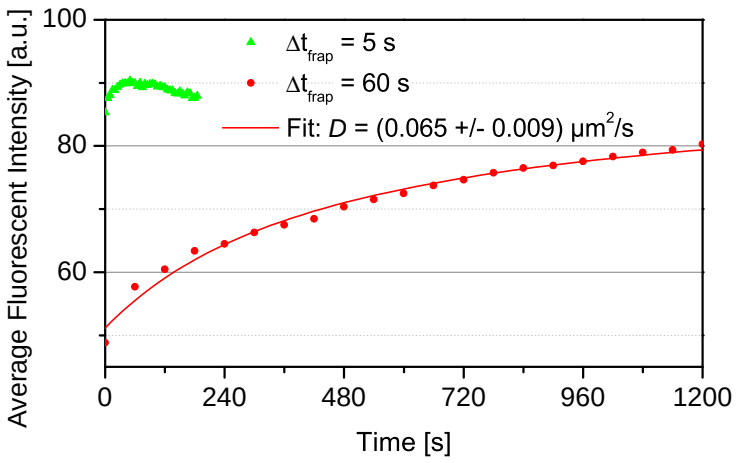

Figure 5.4: FRAP curves of the GFP signal for imaging intervals of 5 and 60 s. For $\Delta t_{frap} = 5\,\mathrm{s}$ fluorescence intensity reached a peak and decreased afterwards. In contrast, for $\Delta t_{frap} = 60\,\mathrm{s}$, the fluorescence intensity increased monotonically, and the data could be fitted using (4.3).

parameters with similar D_{lipid} at $0.6\,\mu\mathrm{m}^2/\mathrm{s}$ and M at 0.8, which correspond to the lipid dye diffusion. In contrast, the kinesin diffusion has D_{kin} around $0.1\,\mu\mathrm{m}^2/\mathrm{s}$ and M from 0.19 to 0.36. Thereby, the values for kinesin diffusion are less precise due to the low fluorescence intensity of the GFP-signal and the consequently large error of the fit parameters. On average, the resulting values for D_{kin} are about 6 times smaller than the according lipid dye diffusion constants D_{lipid}.

Kinesin Diffusion Studied by Single Particle Tracking

For single molecule imaging, it was necessary to have low densities of kinesin motors at the SLB, so that single particles can be discriminated. Therefore, the kinesin was 100-fold further diluted ($c = 28\,\mathrm{ng/ml}$) before introducing it into the flowcell, where it was attached to an SLB of 1 % biotinylated lipids. The kinesin signal obtained by TIRF microcopy was acquired in stream stacks of 500 frames with a framerate of 10/s. Using the *Fiesta* tracking software, the trace of a kinesin molecule could be determined very precisely, which is exemplarily shown in figure 4.5. Subsequently, the mean square

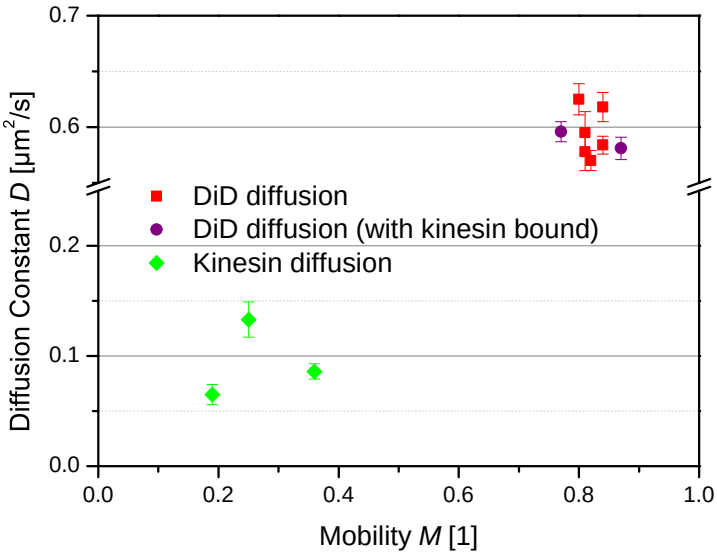

Figure 5.5: Diffusion coefficient and mobile fraction for FRAP of GFP-kinesin (green) and lipid dye diffusion with/without bound kinesin (violet/red), from different channels of one experiment, error bars are standard deviations and result from the individual fit curves. Mean values of the groups are $D_{lipid} = (0.593 \pm 0.012)\ \mu m^2/s$ and $D_{kin} = (0.095 \pm 0.010)\ \mu m^2/s$, whereas the error was determined by error propagation.

displacement $\langle \Delta x^2 \rangle$ was determined for different time intervals Δt_{spt} as it is presented in figure 5.6 for the merged displacements of all tracked molecules from one image stack.

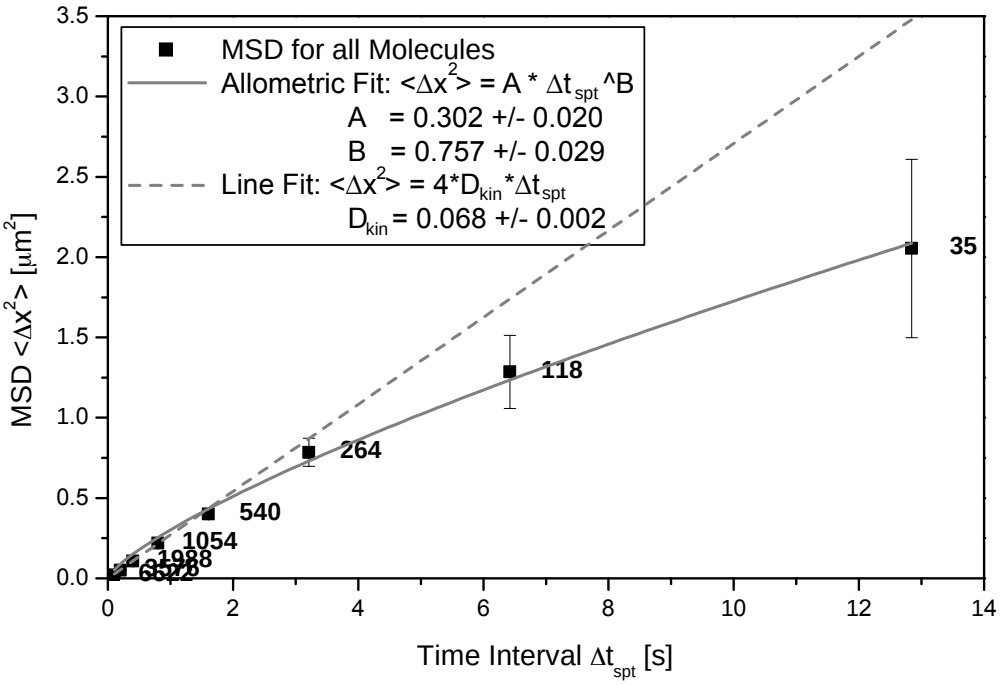

Figure 5.6: Merged mean square displacements of all tracked molecules (70) from one image stack in dependence of time intervals Δt_{spt}. The data points are mean values of the detected displacements with the absolute frequency of occurrence n as indicated by the labels, the error bars represent the standard error of the mean $\sigma_x = \sigma/\sqrt{n}$ of the detected displacements. The functions for the linear and the allometric fit were weighted by n. The linear fit includes the first four data points, the fit data are specified in the boxes.

Assuming pure two-dimensional diffusion, $\langle \Delta x^2 \rangle$ should depend linearly on the time intervals Δt_{spt} as in equation (2.2a). However, the experimental data is better represented using an allometric relation ($\sim \Delta t_{spt}^{\alpha}$) for *anomalous subdiffusion*, which is given by equation (2.2c). That means, the SLB contains areas that are not accessible to the diffusing kinesin. The power of the allometric fit was found to be $\alpha = 0.75 \pm 0.03$, which is not far from pure diffusion ($\alpha = 1$). For short time intervals between the displacements, the diffusion is barely influenced by the subdiffusion, and therefore, the displacements for short intervals ($\Delta t_{spt} = 0.1...0.8\,s$) can be fitted with a linear function. For the first

four data points, this yielded $D_{kin} = (0.068 \pm 0.002)\,\mu m^2/s$.

Further insight into the population of diffusing molecules is provided by the histogram of single molecule diffusion coefficients presented in figure 5.7. The length of trajectories may vary for the different molecules, which affects the frequency of occurrence n of detected displacements and thus the accuracy of individual diffusion constants. Most of the molecules have $D_{kin} < 0.1$ and only few molecules have high diffusion coefficients $D_{kin} > 0.2$.

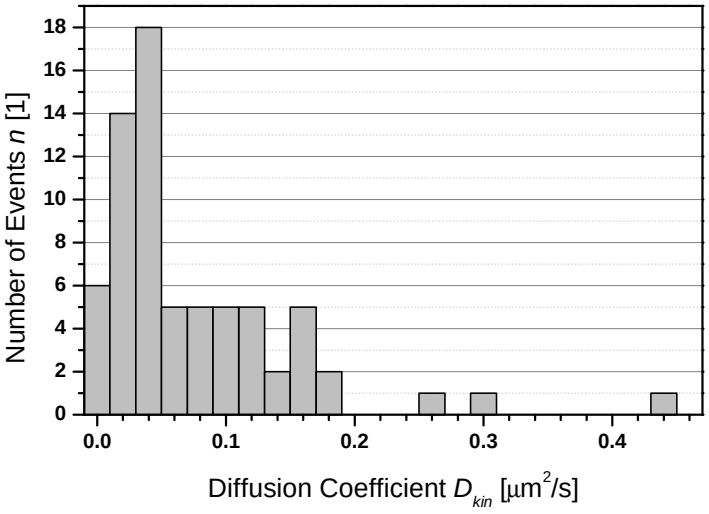

Figure 5.7: Histogram of the diffusion coefficients of single molecules from one image stack. Each D_{kin} was determined from a linear weighted fit of its mean square displacement.

Discussion

Although SLB formation in the flowcell was uncritical when regarding the experiences summarised in section 5.1, inhomogeneities in the SLB increased while flushing in the kinesin-linking components, and it was getting more complicated to guaranty the stability of the SLB. Holes or unruptured vesicles in the SLB are a possible explanation for the anomalous diffusion of kinesin that was found to by SPT. The power of the allometric

fit in a way relates to the mobile fraction in the FRAP method such that $\alpha = 0.75$ corresponds to 75% of the SLB being mobile.

However, it was possible to determine a diffusion coefficient for the kinesin motion from the SPT method using a linear fit of the mean square displacements for short time intervals between the displacements, yielding to $D_{kin}^{spt} = (0.068 \pm 0.002)\,\mu m^2/s$. This value agrees well with number calculated from the FRAP measurements, $D_{kin}^{frap} = (0.095 \pm 0.029)\,\mu m^2/s$, i.e. the methods support each others results.

Furthermore, both methods revealed diffusion coefficients for the kinesin anchored to the SLB smaller than $D_{lipid} = (0.593 \pm 0.012)\,\mu m^2/s$. This was expected, since the kinesin with its SLB anchoring complex must have a lower mobility (and hence smaller D) than the pure lipid dye molecule in the SLB (see also section 3.2). Even the highest D_{kin} for a single molecule value is still smaller than the measured D_{lipid}.

However, the ratio of the diffusion coefficients for pure lipid diffusion and kinesin diffusion D_{kin}/D_{lipid} does not fit to the prediction ($D_{kin}/D_{lipid} = 2/3$, section 3.2), for neither of the methods. Adjusting (3.11) for the experimental diffusion coefficient, shifts the expected ratio D_{kin}/D_{lipid} towards 1, which means that the diffusion of the kinesin linker in the solution has only little impact on the kinesin diffusion. This is a contradiction to the low kinesin diffusion coefficients that have been observed. Even related to the measured D_{lipid}, D_{kin} is reduced by a factor of 6 for FRAP and 10 for SPT, respectively. To explain the discrepancy, several possibilities have to be taken into account:

- The kinesin diffusion in the SLB in somehow hindered. The few fast molecules might represent the freely diffusing kinesin and the others could have further interactions, either with the SLB, e.g. because they are attached to a neutravidin cluster, or with the surface, or with unruptured vesicles at the surface.
- There is an error in the assumption of the STOKES friction in the solution, due to the near surface. Viscous drag forces are higher close to surfaces.
- Although unlikely, both methods may fail: FRAP due to the simplified bleaching method (discussed in the previous section) and SPT because of the error committed by the linear fit of $\langle \Delta x^2 \rangle$ for data points with small Δt_{spt}.

5.3 Microtubule Motility Measurements

Gliding Assay with Fixed Kinesin

The *antibody gliding assay*, where the kinesin is rigidly attached to the surface (see also figure 1.1b), was used to give a reference value for the microtubule gliding velocity of the truncated GFP-kinesin construct under the assay conditions used. Thereby, the impact of using PBS buffer was studied in particular. The microtubule gliding motility was imaged and the velocity of single microtubules was determined as described in section 4.3. In agreement with the theory, a variation of the density of kinesin rigidly attached to the surface caused a change in the surface affinity of the microtubules, but it did *not* affect the gliding velocities. The latter fact is shown in figure 5.8 for an antibody gliding assay in PBS buffer.

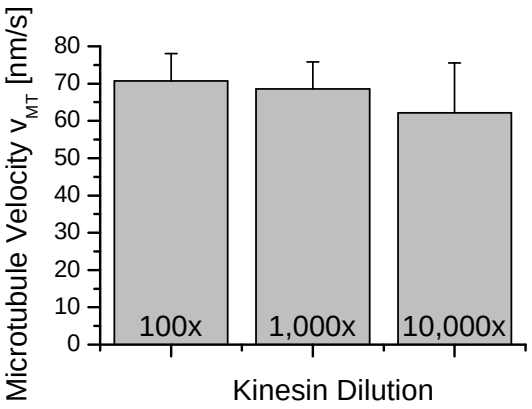

Figure 5.8: Antibody gliding assay in PBS buffer with varying amounts of kinesin at the surface, indicated by the dilution factor, error bars represent the standard error of each population consisting of at least 15 microtubules.

In contrast, the application of different buffers was found to influence the microtubule gliding velocity. Figure 5.9 shows the data for an antibody gliding assay, which had been set up in BRB80. Subsequent washing with PBS motility solution slowed down the velocity from about 400 nm/s to 125 nm/s (later 65 nm/s), and a further flush of BRB80 motility solution was able to revive microtubule speeds. The motility was repeated

several times reproducing the original velocity values[3]. Thereby, it did not matter in which buffer the assay had been set up. The average gliding velocity of 125 mn/s after the first PBS wash (2) was higher than expected for PBS under these conditions, which might be caused by a previous incomplete buffer exchange.

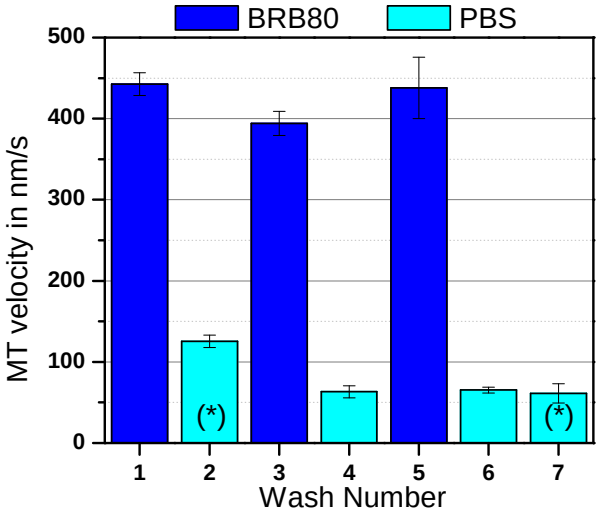

Figure 5.9: Microtubule gliding velocities in the antibody gliding assay for several buffer exchanges in one and the same channel set up in BRB80, error bars represent the standard deviation of 10 evaluated microtubules, (*) indicates PBS with additional 1 mM EGTA.

The reproducibility of the velocities independent from the original buffer confirmed, that the function of the motor proteins is not harmed by the PBS buffer, although the gliding velocity was reduced in PBS compared to BRB80. The low gliding velocities in PBS can be explained by a decreased ATP hydrolysis rate caused by the amount of phosphate in the PBS buffer, which slows down phosphate release from the kinesin motor domain [Schief et al., 2004].

[3]The additional EGTA in the PBS buffer is not supposed to influence the microtubule velocity.

Gliding Assay with Membrane-Anchored Kinesin

Following the protocol from section 4.2, gliding assays on SLB anchored kinesin were performed. Different concentrations of the lipid anchor in the SLB (DSPE-PEG-biotin) have been used in order to control the amount of kinesin at the bilayer surface. Furthermore, it was noted that the variation of motor density on the SLB can also be realised using a fixed concentration of lipid anchor in the SLB but different kinesin concentrations below the saturation threshold. This facilitates the variation of the kinesin density over various orders of magnitude. The results presented in the following were derived from experiments that had been realised in PBS continuously during all steps, since the best stability of the SLB was achieved in this buffer.

Just like for the diffusion of kinesin, the results have to be distinguished with respect to the amount of kinesin at the surface. For low concentrations at single molecule level, there were no binding events of microtubules to the kinesin at the surface. Thus, gliding velocities could not be determined at single molecule kinesin concentrations.

Instead, high kinesin densities at the SLB enabled microtubule binding and motility. The measured microtubule gliding velocities are shown in figure 5.10a, in comparison to the gliding velocities of the control experiments using the antibody gliding assay.

To investigate the dependency of v_{MT} from the microtubule length L at constant motor density, the gliding velocities of single microtubules (figure 5.10a) were linearly fitted for each population. The velocity/length-coefficient of the fit is shown in figure 5.10b for each population. For the high motor density as well as for the control, there was no dependency of v_{MT} on L. For the low motor density, the slope is significantly different from zero (probability $p < 0.05$), although the value of 0.1 nm/s per 1 µm of the microtubule length is very small. According to this, the gliding velocities of each population were averaged, which is presented in figure 5.10c. In the membrane-anchored gliding assay, the gliding velocities were decreased to 46 ± 6 nm/s for the bilayer containing 1 mol% biotinylated lipids and to 31 ± 4 nm/s in case of the bilayer comprising only 0.1 mol% biotinylated lipids, compared the control (69 ± 7 nm/s). This equals a reduction to 67 % and 45 % of the control velocity in the respective cases. It can be assumed, that an increased ratio of biotinylated lipids in the SLB corresponds to a higher density of kinesin at the SLB, and thus to more motors interacting with the microtubule per unit length.

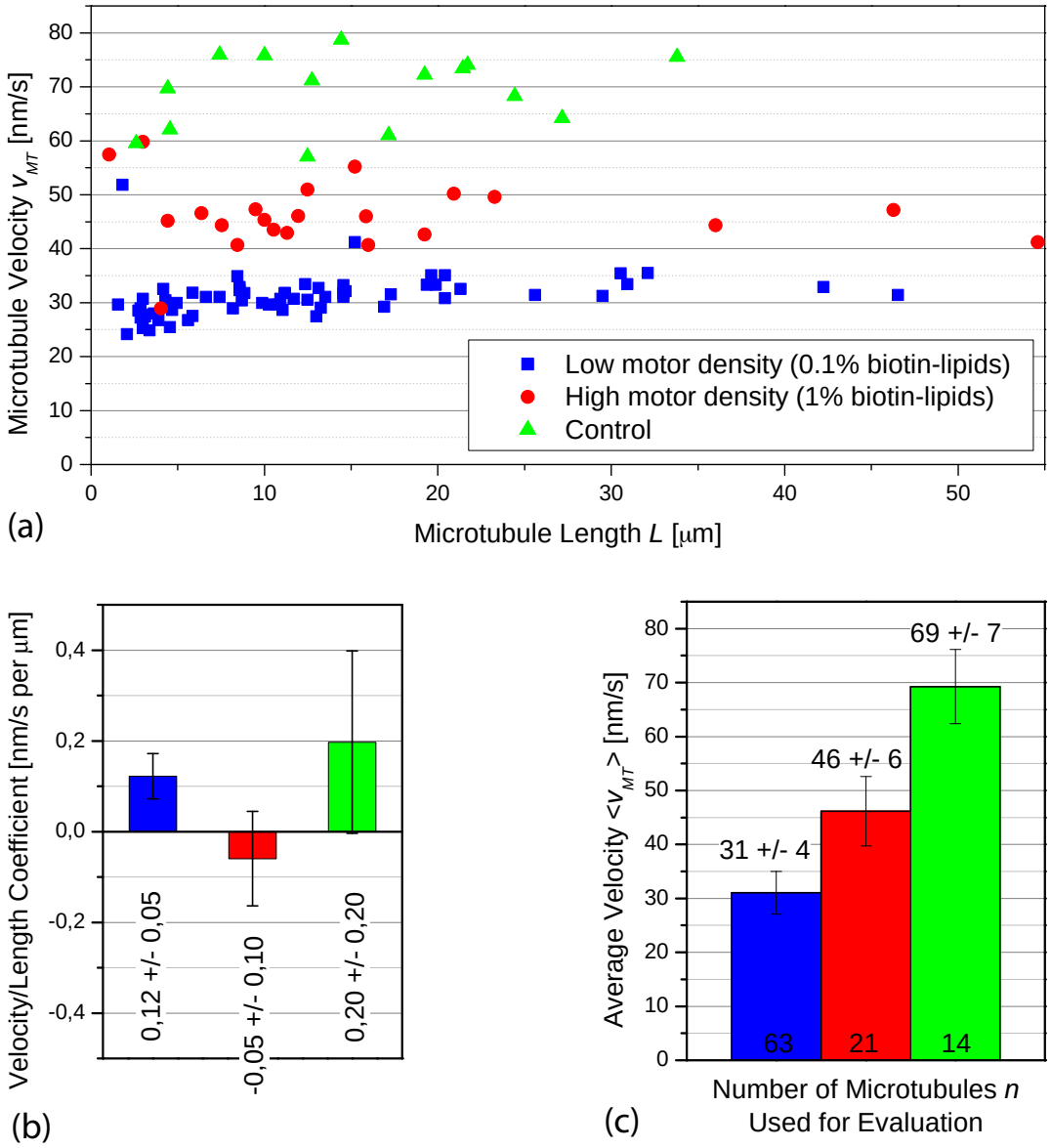

Figure 5.10: Microtubule gliding velocities v_{MT} in the membrane-anchored gliding assay, (a) v_{MT} versus L for motility assays with different amounts of anchor lipids in the SLB that were realised in a parallel manner, compared to the control with fixed kinesin in an antibody gliding assay; (b) velocity/length-coefficient of a linear fit of each population in (a), error bars represent the standard deviation; and (c) average gliding velocities for the three populations, labels show the exact values with the standard deviation, the numbers of microtubules involved in the evaluation are shown at the bottom.

In agreement with the theoretically derived velocity dependence (figure 3.3), v_{MT} was found to increase with the motor density N/L.

Discussion

The experimental data showed, that gliding velocities of microtubules propelled by membrane-anchored kinesin molecules were found to be decreased compared to the control with fixed kinesin. Thereby, it was found that the microtubule gliding velocity did not or only a very slightly depend on the microtubule length. This confirms the statement (i) of the model (see section 3.3).

Furthermore, the velocity increase for higher motor densities at the surface also corresponds to the prediction (ii) of the theoretical model, although there is only qualitative agreement. A quantitative evaluation is not possible, since the number of interacting motor per microtubule could not be determined, due to the high motor densities necessary to achieve microtubule binding, which was impeding single molecule detection.

On the other hand, the theoretical relation between v_{MT} and the motor density N/L predicted by the model can be used for an estimation of the motor density of the two experimental values, as shown in figure 5.11. The motor density at the microtubule can be determined to be 2 and 5 motors/µm in case of the 0.1 % and 1 % biotinylated SLB, respectively. According to that, a microtubule with a length of 20 nm, would be propelled by 40 (or 100) SLB anchored motors for the low (high) motor density, which is a reasonable value.

Considering an average of the experimental values for $D_{kin} = 0.082\,\mu m^2/s$, which were about 40-fold reduced against the results of the model (see section 5.2, assumptions were $D_{lipid} = 5\,\mu m^2/s$, or $D_{kin} = 3\,\mu m^2/s$), the shape of the function $v_{MT}/v_{walk}(N/L)$ would change in a manner that the resulting numbers for the motor density would decrease. The resultant value would most likely better represent the real number of interacting motors.

It can be concluded, that the experimental data in conjunction with the model created a nanometre scale insight into the processes happening during microtubule gliding propelled by membrane-anchored motor proteins.

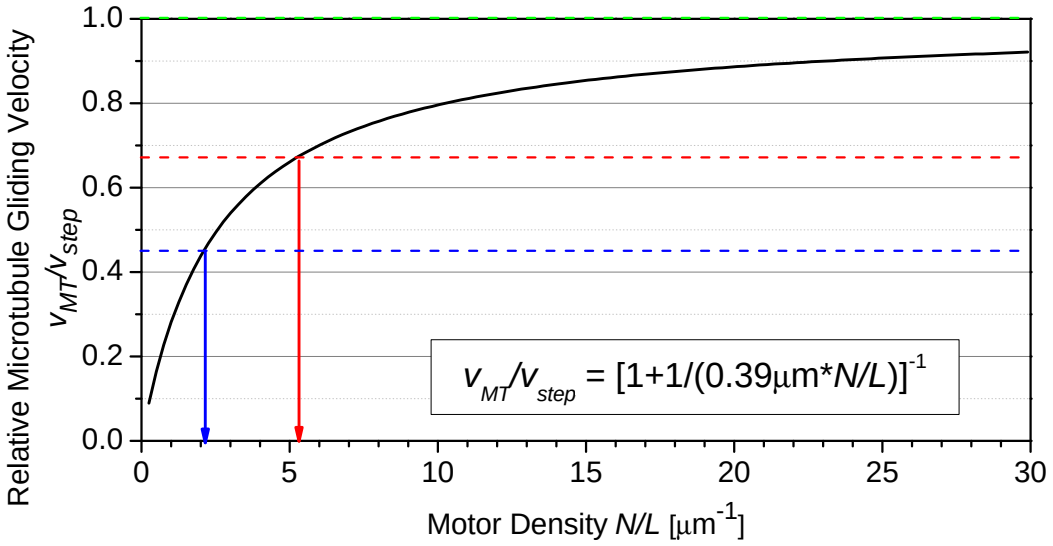

Figure 5.11: Relative microtubule gliding velocity v_{MT}/v_{walk} related to motor density at the microtubule N/L as revealed from the model, introducing the average gliding velocities from the experiment yields the motor density for the two cases.

6 Conclusion and Outlook

Summary

During this thesis, the transport of membrane-bounded cargo carried out by kinesin-1 motor proteins in cells was mimicked *in vitro* using a novel, self-developed membrane-anchored gliding assay. For this purpose, supported lipid bilayers (SLBs) were utilized as a membrane system. Kinesin-1 motors were attached to functionalised lipids in the SLB via a biotin-neutravidin linkage. In this system, microtubule motility driven by the membrane-anchored motor proteins was investigated in theory and experiment. Thereby, the following results were obtained:

- SLBs have been prepared inside a flow chamber, facilitating the exchange of solutions in *in vitro* experiments with motor proteins. The diffusion of the lipids in the SLB was observed using fluorescence recovery after photobleaching (FRAP). From the measurements, the diffusion coefficient was determined to be $D_{lipid} = (0.593 \pm 0.012)\ \mu\text{m}^2/\text{s}$.

- Kinesin-1 motor proteins have been attached to the SLBs. Their diffusion was investigated using the FRAP method as well as single molecule techniques. The evaluation of the experiments yielded diffusion coefficients of $D_{kin}^{frap} = (0.095 \pm 0.010)$ and $D_{kin}^{spt} = (0.068 \pm 0.002)\ \mu\text{m}^2/\text{s}$. For long observation times, the motors were found to undergo anomalous subdiffusion, which was attributed to inhomogeneities in the SLB.

- Microtubule gliding velocities were studied in membrane-anchored gliding assays. Thereby, the gliding velocities were found to be reduced to 66 % (45 %) for very high (medium high) motor densities at the surface, compared to control assays with fixed kinesin. This reduction was attributed to the diffusive anchor in the SLB.

- The system was described theoretically. It revealed that the gliding velocity depends on the number of motors interacting with the microtubule per length, while it is independent from the microtubule length at constant motor density at the surface. This was qualitatively confirmed by the experiments. Furthermore, the model enabled the determination of the number of motors interacting with the microtubule per length of the same from the experiment, yielding reasonable values.

Altogether, it was shown in theory and experiment, that microtubule transport driven by membrane-anchored kinesin-1 is more effective, the more motors interact with the microtubule per unit length. This means that the transport efficiency is coupled to the motor number via the loose coupling of the motors in the membrane, which was imitating the cargo. Thus, the number of motors involved in cargo transport is suggested to be a natural regulator of the efficiency of the transport. To support this outcome and to improve the statistics, the dataset should be enlarged.

Approaches for Future Experiments

The understanding of the present setup could be extended by facilitating the detection of the individual kinesin-1 motors propelling microtubules. Thereby, experimental information about the number of interacting motors could be gained, and compared to the theoretical predictions. During the performed experiments, single molecule detection was impeded by the weak microtubule binding affinity at low motor densities at the SLB. One approach to overcome this problem could be to increase the microtubule binding rate while keeping the motor densities low, however the origin of the low binding rate remains elusive. On the other hand, the motor number could be gained from experiments using a highly concentrated mixture of labelled and unlabelled kinesin motors in a way, that single, labelled motors can be observed at an overall motor density high enough for microtubule binding (*spiking experiments*). This is a nice follow-up experiment that should be easy to realise and that may provide deeper insight into the collective behaviour of the kinesin-1 motors in this membrane associated assembly.

A critical aspect of the presented work is the anomalous subdiffusion of the kinesin molecules in the SLB in conjunction with the evaluation of the microtubule gliding velocities. The theory assumed homogeneous diffusion of the motors at the surface with

a fixed diffusion constant D_{kin}, which was gained from the linear relation between the mean square displacement $\langle \Delta x^2 \rangle$ of a diffusing molecule and the time interval between the displacements Δt_{spt}. However, for anomalous subdiffusion, D_{kin} is related to the time scale at which diffusion is observed by the local slope of $\langle \Delta x^2 \rangle (\Delta t_{spt})$. In the present experiment, the corresponding time frame would be the observation time of the gliding microtubule, i.e. D_{kin} would depend on the observation time of microtubule motility. This would imply drastic changes of the theory that do not target the aim of this work. The emphasis should instead be on the improvement of the quality of the SLB, which was mainly affected by the flush of the binding components into the flowcell.

A possible approach to increase the stability of the SLB could be the exchange of the biotin-neutravidin linkage by a direct membrane anchor, such as Ni-NTA[1] lipids, which are able to establish a direct, dynamic interaction with His-tagged proteins [Dietrich et al., 1996]. However, it has to be tested whether this linker is useful, especially, whether the linkage is strong enough and the dynamics of the binding are slow enough for the application in this assay.

Besides, the membrane-anchored gliding assay has a high potential as an *in vitro* method for the investigation of less well understood motor proteins with respect to their kinetics and collective behaviour. Therefore, members of the kinesin-3 subfamily could be particularly interesting, since they possess a special PH- or PX-domain[2] in the tail region, enabling them to insert directly into phosphatidylinositol-containing membranes [Klopfenstein et al., 2002, Hoepfner et al., 2005].

Concluding Remarks

Studying kinesin-1 and other motor proteins enriches the understanding of active transport in cells. Knowledge of life processes again is essential for a comprehension of health defects, such as Alzheimer's disease, and a basis for the development of medical treatments.

[1] Nitrilotriacetic acid, a chelating acid, i.e. it has two or more separate bindings between a multiple-bonded ligand and a single central atom.

[2] Both, the PX (phox) domain and the PH (pleckstrin homology) domain, are a phosphoinositide-binding, structural protein regions with a lipophilic hook.

Thereby, biological investigations have reached a length scale small enough to study single molecules like kinesin-1 motor proteins. However, from a physical point of view, research usually takes place in (sub-)atomic magnitudes and a single kinesin-1 molecule comprising several thousands of atoms appears extremely complex. Physics and biology are two scientific fields that seem to have drifted apart over the course of their history. Now, actual research creates a new overlap zone in investigation of life processes at the nanometre scale. Here, physicists and biologists in a way approach from opposite sides of the length scale, to proceed with joined forces towards the decryption of the miracles of nature.

Bibliography

[Alberts et al., 2008] Alberts, B., Johnson, A., Lewis, J., Raff, M., Roberts, K., and Walter, P. (2008). *Molecular biology of the cell. Fifth edition.*, volume 5. Garland Science; New York and Oxford.

[Andreu et al., 1992] Andreu, J. M., Bordas, J., Diaz, J. F., García de Ancos, J., Gil, R., Medrano, F. J., Nogales, E., Pantos, E., and Towns-Andrews, E. (1992). Low resolution structure of microtubules in solution. synchrotron x-ray scattering and electron microscopy of taxol-induced microtubules assembled from purified tubulin in comparison with glycerol and map-induced microtubules. *J Mol Biol*, 226(1):169–84.

[Asbury et al., 2003] Asbury, C. L., Fehr, A. N., and Block, S. M. (2003). Kinesin moves by an asymmetric hand-over-hand mechanism. *Science*, 302(5653):2130–4.

[Axelrod et al., 1976] Axelrod, D., Koppel, D. E., Schlessinger, J., Elson, E., and Webb, W. W. (1976). Mobility measurement by analysis of fluorescence photobleaching recovery kinetics. *Biophys J*, 16(9):1055–1069.

[Baumgart et al., 2007] Baumgart, T., Hunt, G., Farkas, E. R., Webb, W. W., and Feigenson, G. W. (2007). Fluorescence probe partitioning between lo/ld phases in lipid membranes. *Biochim Biophys Acta*, 1768(9):2182–94.

[Beeg et al., 2008] Beeg, J., Klumpp, S., Dimova, R., Gracià, R. S., Unger, E., and Lipowsky, R. (2008). Transport of beads by several kinesin motors. *Biophys J*, 94(2):532–41.

[Benes et al., 2002] Benes, M., Billy, D., Hermens, W. T., and Hof, M. (2002). Muscovite (mica) allows the characterisation of supported bilayers by ellipsometry and confocal fluorescence correlation spectroscopy. *Biol Chem*, 383(2):337–41.

[Bieling et al., 2008] Bieling, P., Telley, I. A., Piehler, J., and Surrey, T. (2008). Processive kinesins require loose mechanical coupling for efficient collective motility. *EMBO Rep*, 9(11):1121–7.

[Block et al., 2003] Block, S. M., Asbury, C. L., Shaevitz, J. W., and Lang, M. J. (2003). Probing the kinesin reaction cycle with a 2d optical force clamp. *Proc Natl Acad Sci USA*, 100(5):2351–6.

[Bray, 2001] Bray, D. (2001). *Cell Movements. From Molecules to Motiliy.*, volume 2. Garland Publishing; New York.

[Brian and McConnell, 1984] Brian, A. A. and McConnell, H. M. (1984). Allogeneic stimulation of cytotoxic t cells by supported planar membranes. *Proc Natl Acad Sci U S A*, 81(19):6159–63.

[Chalfie et al., 1994] Chalfie, M., Tu, Y., Euskirchen, G., Ward, W. W., and Prasher, D. C. (1994). Green fluorescent protein as a marker for gene expression. *Science*, 263(5148):802–5.

[Chen et al., 2006] Chen, Y., Lagerholm, B. C., Yang, B., and Jacobson, K. (2006). Methods to measure the lateral diffusion of membrane lipids and proteins. *Methods*, 39(2):147–53.

[Coy et al., 1999] Coy, D. L., Wagenbach, M., and Howard, J. (1999). Kinesin takes one 8-nm step for each atp that it hydrolyzes. *J Biol Chem*, 274(6):3667–71.

[Dagenbach and Endow, 2004] Dagenbach, E. M. and Endow, S. A. (2004). A new kinesin tree. *J Cell Sci*, 117(Pt 1):3–7.

[Desai and Mitchison, 1997] Desai, A. and Mitchison, T. J. (1997). Microtubule polymerization dynamics. *Annu Rev Cell Dev Biol*, 13:83–117.

[Dietrich et al., 1996] Dietrich, C., Boscheinen, O., Scharf, K. D., Schmitt, L., and Tampé, R. (1996). Functional immobilization of a dna-binding protein at a membrane interface via histidine tag and synthetic chelator lipids. *Biochemistry*, 35(4):1100–5.

[Engelman, 1969] Engelman, D. M. (1969). Surface area per lipid molecule in the intact membrane of the human red cell. *Nature*, 223(5212):1279–80.

[Feder et al., 1996] Feder, T. J., Brust-Mascher, I., Slattery, J. P., Baird, B., and Webb, W. W. (1996). Constrained diffusion or immobile fraction on cell surfaces: a new interpretation. *Biophys J*, 70(6):2767–73.

[Feit et al., 1971] Feit, H., Slusarek, L., and Shelanski, M. L. (1971). Heterogeneity of tubulin subunits. *Proc Natl Acad Sci U S A*, 68(9):2028–31.

[Fujiwara et al., 2002] Fujiwara, T., Ritchie, K., Murakoshi, H., Jacobson, K., and Kusumi, A. (2002). Phospholipids undergo hop diffusion in compartmentalized cell membrane. *J Cell Biol*, 157(6):1071–81.

[Glotzer, 2009] Glotzer, M. (2009). The 3ms of central spindle assembly: microtubules, motors and maps. *Nat Rev Mol Cell Biol*, 10(1):9–20.

[Gorter and Grendel, 1925] Gorter, E. and Grendel, F. (1925). On bimolecular layers of lipoids on the chromocytes of the blood. *J Exp Med*, 41(4):439–443.

[Hackney, 1995] Hackney, D. D. (1995). Highly processive microtubule-stimulated atp hydrolysis by dimeric kinesin head domains. *Nature*, 377(6548):448–50.

[Hayden et al., 1990] Hayden, J. H., Bowser, S. S., and Rieder, C. L. (1990). Kinetochores capture astral microtubules during chromosome attachment to the mitotic spindle: direct visualization in live newt lung cells. *J Cell Biol*, 111(3):1039–45.

[Hirokawa and Noda, 2008] Hirokawa, N. and Noda, Y. (2008). Intracellular transport and kinesin superfamily proteins, kifs: structure, function, and dynamics. *Physiol Rev*, 88(3):1089–118.

[Hirokawa et al., 2009] Hirokawa, N., Noda, Y., Tanaka, Y., and Niwa, S. (2009). Kinesin superfamily motor proteins and intracellular transport. *Nat Rev Mol Cell Biol*, 10(10):682–96.

[Hoepfner et al., 2005] Hoepfner, S., Severin, F., Cabezas, A., Habermann, B., Runge, A., Gillooly, D., Stenmark, H., and Zerial, M. (2005). Modulation of receptor recycling and degradation by the endosomal kinesin kif16b. *Cell*, 121(3):437–50.

[Howard, 2001] Howard, J. (2001). *Mechanics of Motor Proteins and the Cytoskeleton.*, volume 1. Sinauer Associates, Inc.; Sunderland Massachusetts.

[Howard et al., 1989] Howard, J., Hudspeth, A. J., and Vale, R. D. (1989). Movement of microtubules by single kinesin molecules. *Nature*, 342(6246):154–8.

[Hunt et al., 1994] Hunt, A. J., Gittes, F., and Howard, J. (1994). The force exerted by a single kinesin molecule against a viscous load. *Biophys J*, 67(2):766–81.

[Israelachvili, 1992] Israelachvili, J. N. (1992). *Intermolecular and Surface Forces*. Academic Press Limited, London, 2 edition.

[Johnson et al., 2002] Johnson, J. M., Ha, T., Chu, S., and Boxer, S. G. (2002). Early steps of supported bilayer formation probed by single vesicle fluorescence assays. *Biophys J*, 83(6):3371–9.

[Karcher et al., 2002] Karcher, R. L., Deacon, S. W., and Gelfand, V. I. (2002). Motor-cargo interactions: the key to transport specificity. *Trends Cell Biol*, 12(1):21–27.

[Kim and Endow, 2000] Kim, A. J. and Endow, S. A. (2000). A kinesin family tree. *J Cell Sci*, 113 Pt 21:3681–2.

[Kirschner and Mitchison, 1986] Kirschner, M. and Mitchison, T. (1986). Beyond self-assembly: from microtubules to morphogenesis. *Cell*, 45(3):329–42.

[Klopfenstein et al., 2002] Klopfenstein, D. R., Tomishige, M., Stuurman, N., and Vale, R. D. (2002). Role of phosphatidylinositol(4,5)bisphosphate organization in membrane transport by the unc104 kinesin motor. *Cell*, 109(3):347–358.

[Korten and Diez, 2008] Korten, T. and Diez, S. (2008). Setting up roadblocks for kinesin-1: mechanism for the selective speed control of cargo carrying microtubules. *Lab Chip*, 8(9):1441–7.

[Kozielski et al., 1997] Kozielski, F., Sack, S., Marx, A., Thormählen, M., Schönbrunn, E., Biou, V., Thompson, A., Mandelkow, E. M., and Mandelkow, E. (1997). The crystal structure of dimeric kinesin and implications for microtubule-dependent motility. *Cell*, 91(7):985–94.

[Laitinen et al., 2006] Laitinen, O. H., Hytönen, V. P., Nordlund, H. R., and Kulomaa, M. S. (2006). Genetically engineered avidins and streptavidins. *Cell Mol Life Sci*, 63(24):2992–3017.

[Lakowicz, 2006] Lakowicz, J. R. (2006). *Principles of Fluorescence Spectroscopy*, volume 3. Springer Science+Business Media.

[Leduc et al., 2004] Leduc, C., Campàs, O., Zeldovich, K. B., Roux, A., Jolimaitre, P., Bourel-Bonnet, L., Goud, B., Joanny, J.-F., Bassereau, P., and Prost, J. (2004). Cooperative extraction of membrane nanotubes by molecular motors. *Proc Natl Acad Sci U S A*, 101(49):17096–101.

[Leduc et al., 2007] Leduc, C., Ruhnow, F., Howard, J., and Diez, S. (2007). Detection of fractional steps in cargo movement by the collective operation of kinesin-1 motors. *Proc Natl Acad Sci U S A*, 104(26):10847–10852.

[Loose et al., 2008] Loose, M., Fischer-Friedrich, E., Ries, J., Kruse, K., and Schwille, P. (2008). Spatial regulators for bacterial cell division self-organize into surface waves in vitro. *Science*, 320(5877):789–792.

[Mallik and Gross, 2004] Mallik, R. and Gross, S. P. (2004). Molecular motors: strategies to get along. *Curr Biol*, 14(22):R971–82.

[Martin, 2007] Martin, L. (2007). A lipid bilayer model of cell membrane structure.

[Merkel et al., 1999] Merkel, R., Nassoy, P., Leung, A., Ritchie, K., and Evans, E. (1999). Energy landscapes of receptor-ligand bonds explored with dynamic force spectroscopy. *Nature*, 397(6714):50–3.

[Miki et al., 2005] Miki, H., Okada, Y., and Hirokawa, N. (2005). Analysis of the kinesin superfamily: insights into structure and function. *Trends Cell Biol*, 15(9):467–476.

[Nagle and Tristram-Nagle, 2000] Nagle, J. F. and Tristram-Nagle, S. (2000). Structure of lipid bilayers. *Biochim Biophys Acta*, 1469(3):159–95.

[Niehaus et al., 2008] Niehaus, A. M. S., Vlachos, D. G., Edwards, J. S., Plechac, P., and Tribe, R. (2008). Microscopic simulation of membrane molecule diffusion on corralled membrane surfaces. *Biophys J*, 94(5):1551–64.

[Nielsen et al., 1999] Nielsen, M., Miao, L., Ipsen, J. H., Zuckermann, M. J., and Mouritsen, O. G. (1999). Off-lattice model for the phase behavior of lipid-cholesterol bilayers. *Phys Rev E Stat Phys Plasmas Fluids Relat Interdiscip Topics*, 59(5 Pt B):5790–803.

[Nitzsche et al., 2008] Nitzsche, B., Ruhnow, F., and Diez, S. (2008). Quantum-dot-assisted characterization of microtubule rotations during cargo transport. *Nat Nanotechnol*, 3(9):552–556.

[Nowotschin et al., 2009] Nowotschin, S., Eakin, G. S., and Hadjantonakis, A.-K. (2009). Live-imaging fluorescent proteins in mouse embryos: multi-dimensional, multi-spectral perspectives. *Trends Biotechnol*, 27(5):266–76.

[Ray et al., 1993] Ray, S., Meyhöfer, E., Milligan, R. A., and Howard, J. (1993). Kinesin follows the microtubule's protofilament axis. *J Cell Biol*, 121(5):1083–93.

[Reviakine and Brisson, 2000] Reviakine, I. and Brisson, A. (2000). Formation of supported phospholipid bilayers from unilamellar vesicles investigated by atomic force microscopy. *Langmuir*, 16(4):1806–1815.

[Richter et al., 2006] Richter, R. P., Berat, R., and Brisson, A. R. (2006). Formation of solid-supported lipid bilayers: an integrated view. *Langmuir*, 22(8):3497–3505.

[Rizzuto et al., 1995] Rizzuto, R., Brini, M., Pizzo, P., Murgia, M., and Pozzan, T. (1995). Chimeric green fluorescent protein as a tool for visualizing subcellular organelles in living cells. *Curr Biol*, 5(6):635–42.

[Rogers et al., 2001] Rogers, K. R., Weiss, S., Crevel, I., Brophy, P. J., Geeves, M., and Cross, R. (2001). Kif1d is a fast non-processive kinesin that demonstrates novel k-loop-dependent mechanochemistry. *EMBO J*, 20(18):5101–13.

[Sackmann, 1996] Sackmann, E. (1996). Supported membranes: scientific and practical applications. *Science*, 271(5245):43–8.

[Schief et al., 2004] Schief, W. R., Clark, R. H., Crevenna, A. H., and Howard, J. (2004). Inhibition of kinesin motility by adp and phosphate supports a hand-over-hand mechanism. *Proc Natl Acad Sci U S A*, 101(5):1183–8.

[Schiff et al., 1979] Schiff, P. B., Fant, J., and Horwitz, S. B. (1979). Promotion of microtubule assembly in vitro by taxol. *Nature*, 277(5698):665–7.

[Schnitzer and Block, 1997] Schnitzer, M. J. and Block, S. M. (1997). Kinesin hydrolyses one atp per 8-nm step. *Nature*, 388(6640):386–90.

[Schönherr et al., 2004] Schönherr, H., Johnson, J. M., Lenz, P., Frank, C. W., and Boxer, S. G. (2004). Vesicle adsorption and lipid bilayer formation on glass studied by atomic force microscopy. *Langmuir*, 20(26):11600–6.

[Schwille et al., 1999] Schwille, P., Korlach, J., and Webb, W. W. (1999). Fluorescence correlation spectroscopy with single-molecule sensitivity on cell and model membranes. *Cytometry*, 36(3):176–82.

[Scomparin et al., 2008] Scomparin, C., Lecuyer, S., Ferreira, M., Charitat, T., and Tinland, B. (2008). Diffusion in supported lipid bilayers: Influence of substrate and preparation technique on the internal dynamics. *Eur Phys J E Soft Matter*.

[Seu et al., 2007] Seu, K. J., Pandey, A. P., Haque, F., Proctor, E. A., Ribbe, A. E., and Hovis, J. S. (2007). Effect of surface treatment on diffusion and domain formation in supported lipid bilayers. *Biophys J*, 92(7):2445–50.

[Shubeita et al., 2008] Shubeita, G. T., Tran, S. L., Xu, J., Vershinin, M., Cermelli, S., Cotton, S. L., Welte, M. A., and Gross, S. P. (2008). Consequences of motor copy number on the intracellular transport of kinesin-1-driven lipid droplets. *Cell*, 135(6):1098–107.

[Simons and Ikonen, 1997] Simons, K. and Ikonen, E. (1997). Functional rafts in cell membranes. *Nature*, 387(6633):569–72.

[Sonnleitner et al., 1999] Sonnleitner, Schutz, and Schmidt (1999). Free brownian motion of individual lipid molecules in biomembranes. *Biophys J*, 77(5):2638–42.

[Stowers et al., 2002] Stowers, R. S., Megeath, L. J., Górska-Andrzejak, J., Meinertzhagen, I. A., and Schwarz, T. L. (2002). Axonal transport of mitochondria to synapses depends on milton, a novel drosophila protein. *Neuron*, 36(6):1063–77.

[Svoboda and Block, 1994] Svoboda, K. and Block, S. M. (1994). Force and velocity measured for single kinesin molecules. *Cell*, 77(5):773–84.

[Svoboda et al., 1993] Svoboda, K., Schmidt, C. F., Schnapp, B. J., and Block, S. M. (1993). Direct observation of kinesin stepping by optical trapping interferometry. *Nature*, 365(6448):721–7.

[Toyoshima et al., 1992] Toyoshima, I., Yu, H., Steuer, E. R., and Sheetz, M. P. (1992).

Kinectin, a major kinesin-binding protein on er. *J Cell Biol*, 118(5):1121–31.

[Vale et al., 1985] Vale, R. D., Schnapp, B. J., Mitchison, T., Steuer, E., Reese, T. S., and Sheetz, M. P. (1985). Different axoplasmic proteins generate movement in opposite directions along microtubules in vitro. *Cell*, 43(3 Pt 2):623–32.

[Vist and Davis, 1990] Vist, M. R. and Davis, J. H. (1990). Phase equilibria of cholesterol/dipalmitoylphosphatidylcholine mixtures: 2h nuclear magnetic resonance and differential scanning calorimetry. *Biochemistry*, 29(2):451–64.

[Wade, 2009] Wade, R. H. (2009). On and around microtubules: an overview. *Mol Biotechnol*, 43(2):177–91.

[Yildiz et al., 2008] Yildiz, A., Tomishige, M., Gennerich, A., and Vale, R. D. (2008). Intramolecular strain coordinates kinesin stepping behavior along microtubules. *Cell*, 134(6):1030–41.

[Yildiz et al., 2004] Yildiz, A., Tomishige, M., Vale, R. D., and Selvin, P. R. (2004). Kinesin walks hand-over-hand. *Science*, 303(5658):676–8.

Acknowledgements

Now that I have managed, I want to express my gratitude to many people that contributed to this work in whatever kind of way and without their support I would not have managed.

Foremost, I want to thank Dr. Stefan Diez, for giving me the opportunity to work in such a kind environment of interdisciplinary scientists and friends, that was deepening my fascination for the world of molecular motors while getting to know the experimental challenges of research at the nanometre scale. Thank you for your catching enthusiasm and your support.

Prof. Petra Schwille and Prof. Jonathon Howard for their cooperation, especially Prof. Schwille for enabling the collaboration with the BIOTEC.

In this context, I want to point out Christoph Herold, who taught me the basics of SLB formation and spent his time debugging the problems that I had.

To the members of the Diez-lab I am thankful for the fruitful discussions, lunch talks and funny lab-retreats. Especially: Till and René, for many hints and critical comments during the lab work and while writing. Gero and Bert, for their useful experimental advises. Felix, who can never ever be substituted by any tracking software handbook. Corina and Cordula, my female labmates, it was a pleasure having you around. Thank you, Veikko, for the motivating discussions of scientific and philosophical questions. Thanks, Claudi, for the very personal exchange under diploma students.

All the patient readers of my manuscript may feel invited for some ice-cream, or maybe you can pay me back with your own manuscript... ;)

Von ganzem Herzen möchte ich mich bei meiner Familie bedanken, insbesondere bei meinen Eltern, meinem Opa und meinem Bruder, für die finanzielle und moralische

Unterstützung auf meinem Lebensweg, ohne die ich jetzt nicht da wäre, wo ich bin. Danke für selbstgemachte Marmelade, Sportleidenschaft und Umzugshilfen.

Unas gracias castellanos andan alrededor de la mitad del mundo, hacia Eugenio Vogel en Temuco. Hizo posible una estancia excitante e inolvidable, que me ha marcado profundamente.

Finally, I am very grateful to my friends, for sharing happiness and sadness, for together listening, laughing and realising crazy ideas. How could I have a (physical) conversation on my own, or play table-tennis or volleyball? And, I would actually not *want* to eat the whole cake alone... Thank you. You are the driving force and the equilibrium in my life.